TR-8643
0012

NUSC Technical Report 8643
18 October 1989

Analysis and Design of a Loran-C Antenna

Dr. John P. Casey
Submarine Electromagnetic Systems Department

Dr. Rajeev Bansal
University of Connecticut

Naval Underwater Systems Center
New London, Connecticut / Newport, Rhode Island

Preface

This work was conducted under the NUSC Submarine Antenna R&D Program; Program Manager, A. R. Susi, Code 34292.

The technical reviewer for this report was Kurt F. Hafner.

Acknowledgments

The authors would like to thank Mr. Charles Odams and Mr. Kurt Hafner of the Antenna Systems Branch for many helpful discussions. In addition, special thanks are extended to Mr. David Esterquest of the Antenna Systems Branch for taking the capacitance measurements and to Mr. Gabriel Silberman for preparing some of the figures.

Reviewed and Approved: 18 October 1989

D. F. Dence
Head, Submarine Electromagnetic
Systems Department

Dr. Casey is located at the New London Laboratory,
Naval Underwater Systems Center,
New London, Connecticut 06320

Dr. Bansal is with the Department of Electrical and Systems Engineering,
University of Connecticut,
Storrs, Connecticut 06269

REPORT DOCUMENTATION PAGE

1a. REPORT SECURITY CLASSIFICATION	1b. RESTRICTIVE MARKINGS
Unclassified	

2a. SECURITY CLASSIFICATION AUTHORITY	3. DISTRIBUTION / AVAILABILITY OF REPORT
	APPROVED FOR PUBLIC RELEASE; DISTRIBUTION UNLIMITED
2b. DECLASSIFICATION / DOWNGRADING SCHEDULE	

4. PERFORMING ORGANIZATION REPORT NUMBER(S)	5. MONITORING ORGANIZATION REPORT NUMBER(S)
TR 8643	

6a. NAME OF PERFORMING ORGANIZATION	6b. OFFICE SYMBOL (If applicable)	7a. NAME OF MONITORING ORGANIZATION
NAVAL UNDERWATER SYSTEMS CENTER		

6c. ADDRESS (City, State, and ZIP Code)	7b. ADDRESS (City, State, and ZIP Code)
NEW LONDON LABORATORY NEW LONDON, CT 06320-5594	

8a. NAME OF FUNDING / SPONSORING ORGANIZATION	8b. OFFICE SYMBOL (If applicable)	9. PROCUREMENT INSTRUMENT IDENTIFICATION NUMBER

8c. ADDRESS (City, State, and ZIP Code)	10. SOURCE OF FUNDING NUMBERS			
	PROGRAM ELEMENT NO.	PROJECT NO.	TASK NO.	WORK UNIT ACCESSION NO.

11. TITLE (Include Security Classification)

ANALYSIS AND DESIGN OF A LORAN-C ANTENNA (U)

12. PERSONAL AUTHOR(S)

DR. JOHN CASEY, DR. RAJEEV BANSAL

13a. TYPE OF REPORT	13b. TIME COVERED FROM _____ TO _____	14. DATE OF REPORT (Year, Month, Day) 89/10/18	15. PAGE COUNT

16. SUPPLEMENTARY NOTATION

17. COSATI CODES			18. SUBJECT TERMS (Continue on reverse if necessary and identify by block number)
FIELD	GROUP	SUB-GROUP	LORAN-C BODY OF REVOLUTION
			MONOPOLE ANTENNA METHOD OF MOMENTS
			QUASI STATIC EFFECTIVE HEIGHT

19. ABSTRACT (Continue on reverse if necessary and identify by block number)

A theoretical analysis of an optimum antenna configuration for Loran-C reception that fits within certain alloted space requirements is given. The antenna analysis is based on a quasi-static numerical study of a conducting body of revolution above a perfectly conducting ground plane. A general numerical algorithm is developed to determine the input impedance and effective height of the antenna. In addition, a discussion of the amplifier noise and its role in the choice of the optimum antenna are given. Results are presented for cylindrical and truncated conical structures both with and without a top load.

20. DISTRIBUTION / AVAILABILITY OF ABSTRACT	21. ABSTRACT SECURITY CLASSIFICATION
☐ UNCLASSIFIED/UNLIMITED ☐ SAME AS RPT. ☐ DTIC USERS	UNCLASSIFIED

22a. NAME OF RESPONSIBLE INDIVIDUAL	22b. TELEPHONE (Include Area Code)	22c. OFFICE SYMBOL
DR. JOHN P. CASEY	(203)440-5388	

DD FORM 1473, 84 MAR

83 APR edition may be used until exhausted.
All other editions are obsolete.

TABLE OF CONTENTS

LIST OF ILLUSTRATIONS

LIST OF ILLUSTRATIONS (Cont'd)

INTRODUCTION

NUSC has been involved in the development of a Loran-C antenna and preamplifier/ matching network that is compatible with a commercial GPS antenna and navigation receiver. To be compatible with the navigation receiver, the Loran antenna must be linearly polarized and provide omni-azimuthal reception at the operational 100 kHz carrier frequency with a 20 kHz bandwidth. In addition, the Loran antenna is electrically small since it is designed to fit within a cylindrical volume of maximum height between 4 and 8 in. and maximum diameter between 3 and 8 in. The restrictions on the maximum dimensions of the antenna were set during the analysis stage of the design. The Loran-C/GPS package is designed to be placed on a floating platform. Fig. 1 gives a block diagram of the Loran-C/GPS integrated antenna system.

This report is primarily concerned with the theoretical determination of an optimum antenna for Loran-C reception that fits within the allowable dimensions. This study includes an analysis of the amplifier noise along with a determination of the input reactance and the effective height of the antenna. The analysis is restricted to monopole antennas since a constant amplitude and phase response is required for all azimuthal angles. Wherever possible, the theoretical models are validated by experimental data.

CIRCUIT ANALYSIS

Consider an electrically short monopole of height h above a ground plane as shown in Fig. 2a. The Thevenin equivalent circuit of the monopole receiving a signal is given in Fig. 2b, where

V_{oc} = open circuit voltage received by the antenna,

R_a = radiation resistance of the antenna,

R_l = ohmic resistance of the antenna,

C_a = antenna capacitance.

R_l includes the ohmic losses associated with the finite conductivities of the antenna and the sea water ground plane. Since the loss tangent in sea water is very large over the frequency range of

1

concern, the ground plane may be approximated by a perfect conductor. The input impedance of the monopole antenna is $R + 1/j\omega C_a$, where ω is the angular frequency while $R = R_a + R_l$ and $R << 1/j\omega C_a$. The antenna capacitance is obtained by solving an electrostatics problem [1]. In the limiting case of a vanishingly small frequency, a dipole or monopole antenna is just a capacitor. For a uniform incident electric field E^{inc} directed parallel to and in the vicinity of the antenna, the open circuit voltage is given by [2]

$$V_{oc} = E^{inc} \, h_{eff} \tag{1}$$

where h_{eff} is the effective height of the antenna. The computation of the antenna capacitance and effective height will be discussed later.

Next consider the monopole connected by a short wire to the input of an FET amplifier as shown in Fig. 3a with equivalent circuit given in Fig. 3b, where

C_w = interconnection capacitance between the antenna and the amplifier,

R_o = input resistance of the amplifier,

C_o = input capacitance of the amplifier,

V_n = open circuit noise voltage produced by the amplifier

To compare the total noise produced by the amplifier with the atmospheric noise received by the antenna, all voltages must be referred to the same location. For convenience, we will refer all noise voltages to the antenna terminals. The thermal noise voltage associated with the loss resistance R_l of the antenna has been computed to be of negligible value and will not be considered further in this analysis.

To determine the amplifier noise, consider Figs. 4(a) and 4(b). The voltage E_n and current I_n are equivalent noise sources that adequately represent the noise produced by the amplifier and whose values can easily be determined experimentally [3]. The total noise power produced by the amplifier is given by the sum of the contributions from E_n and I_n. V_{i1} is the voltage produced by E_n at the input terminals of the amplifier while V_{i2} is the voltage produced by I_n at the same location. Y_a, Y_w, and Y_o are the admittances of the antenna, the interconnection, and the amplifier, respectively. An analysis of Figs. 4(a) and 4(b) yields

2

$$V_{i1} = E_n \left(\frac{Y_a + Y_w}{Y_a + Y_w + Y_o} \right) \tag{2a}$$

$$V_{i2} = I_n \left(\frac{1}{Y_a + Y_w + Y_o} \right) \tag{2b}$$

V_{i1} and V_{i2} can be referred to equivalent sources at the antenna terminals by considering Fig. 5. In Fig. 5, a voltage source V_s at the antenna terminals produces a voltage V_{is} at the input of the amplifier. An analysis of Fig. 5 yields

$$K_v = \frac{V_{is}}{V_s} = \frac{Y_a}{Y_a + Y_w + Y_o} \tag{3}$$

where K_v is the voltage transfer function. The application of (3) to (2a) and (2b) gives the equivalent amplifier noise voltage sources V_{n1} and V_{n2} due to E_n and I_n, respectively, at the antenna terminals. Therefore, from (2) and (3),

$$V_{n1} = \frac{V_{i1}}{K_v} = E_n \left(1 + \frac{Y_w}{Y_a} \right) \tag{4a}$$

$$V_{n2} = \frac{V_{i2}}{K_v} = I_n \frac{1}{Y_a} \tag{4b}$$

If V_{n1} and V_{n2} are uncorrelated, the open-circuit noise voltage V_n produced by the amplifier is given by

$$V_n = \left(|V_{n1}|^2 + |V_{n2}|^2 \right)^{1/2}$$

$$= \left[|E_n|^2 \left| 1 + \frac{Y_w}{Y_a} \right|^2 + |I_n|^2 \left| \frac{1}{Y_a} \right|^2 \right]^{1/2} \tag{5}$$

Note that V_n is independent of the amplifier impedance.

For convenience, we may relate the amplifier noise voltage to an equivalent incident electric

field through the effective height of the receiving antenna. From (1) and (5),

$$E^{amp} = \frac{V_n}{h_{eff}} = \frac{1}{h_{eff}} \left[|E_n|^2 \left| 1 + \frac{Y_w}{Y_a} \right|^2 + |I_n|^2 \left| \frac{1}{Y_a} \right|^2 \right]^{1/2} \tag{6}$$

E^{amp} is the incident electric field parallel to the antenna that produces the same noise power as the amplifier. The substitution of $Y_a \cong j\omega C_a$ and $Y_w = j\omega C_w$ into (6) gives

$$E^{amp} \cong \frac{1}{h_{eff}} \left[|E_n|^2 \left(1 + \frac{C_w}{C_a} \right)^2 + |I_n|^2 \left(\frac{1}{\omega C_a} \right)^2 \right]^{1/2} \tag{7}$$

The goal of this effort is to design an antenna that produces a minimum value of E^{amp}. Therefore, it is desirable to maximize both the antenna capacitance and the effective height. This requirement results in a tradeoff that will be discussed later. It is preferred that the antenna/amplifier system be atmospheric noise limited; i.e., $E^{amp} < E^{atm}$, where E^{atm} is the atmospheric noise field as determined from the CCIR manual [4].

ANTENNA CAPACITANCE

The electrostatic charge distribution and capacitance of an electrically small antenna play an important role in determining its circuit and radiation characteristics. No analytical expression exists for the charge distribution along an arbitrary conducting body of finite dimensions in free space or over a ground plane. This section presents a numerical algorithm for determining the electrostatic charge density distribution and capacitance of a conducting body of revolution above a perfectly conducting ground plane. The algorithm is applied to the analysis of several monopole antenna geometries including cylinders and truncated cones. Each structure will be studied both with and without a top load. The algorithm is verified by comparing the computed capacitances of various cylinders with measured data.

INTEGRAL EQUATION FORMULATION

Consider a body of revolution which is formed by rotating a planar curve about the z-axis as

described in Fig. 6. In Fig. 6, (ρ,ϕ,z) are cylindrical coordinates, and (t,ϕ) form an orthogonal curvilinear coordinate system on the surface S of the body of revolution. The coordinate t is the arc-length along the generating curve and ϕ is the azimuthal angle measured from the x-z plane. The ends of the generating curve may touch the z-axis.

If the body of revolution is a conductor charged to a potential V with respect to a ground plane located on the x-y plane, the following integral equation for the unknown surface charge density σ_s results [1]:

$$\frac{1}{4\pi\varepsilon_0} \iint \sigma_s(\mathbf{r'})\left(\frac{1}{R^+} - \frac{1}{R^-}\right) dS' = V \qquad \mathbf{r} \in S \qquad (8)$$

where $\mathbf{r}$ and $\mathbf{r'}$ are position vectors of the observation and source points, respectively, and the integration is over the surface of the body. In (8), R^+ and R^- denote the distances between the observation and source points on the body and its image, respectively. Since the boundary conditions and excitation are axisymmetric, all field quantities are ϕ-independent. Therefore, ϕ may be set equal to zero and suppressed. In the coordinate system of the surface of revolution, (8) may be expressed as

$$\frac{1}{4\pi\varepsilon_0} \int_0^T \int_{-\pi}^{\pi} \sigma_s(t')\left(\frac{1}{R^+} - \frac{1}{R^-}\right)\rho'(t')\,d\phi'\,dt' = V \qquad \mathbf{r} \in S \qquad (9)$$

where

$$dt' = [\,(d\rho')^2 + (dz')^2\,]^{1/2} \qquad (10)$$

$$R^\pm = |\mathbf{r} \mp \mathbf{r'}| = \left[\,(\rho - \rho')^2 + (z \mp z')^2 + 4\rho\rho'\sin^2\frac{\phi'}{2}\,\right]^{1/2} \qquad (11)$$

T is the total arc length along the generating curve. The unprimed coordinates refer to the observation point while the primed coordinates refer to the source points. Note that ρ and z can be expressed as functions of t where (ρ,z) and (ρ',z') are the cylindrical coordinates of the points t and t', respectively.

Since the surface charge density is axisymmetric, we may write

$$q(t') = 2\pi\rho(t')\sigma_s(t') \tag{12}$$

where q(t) is the linear charge density. The substitution of (12) into (9) gives

$$\frac{1}{4\pi^2\varepsilon_0}\int_0^T q(t')\left[\int_0^\pi \left(\frac{1}{R^+} - \frac{1}{R^-}\right)d\phi'\right]dt' = V \tag{13}$$

Note that the even symmetry of the integrand with respect to $\phi' = 0$ has been accounted for in (13). The substitution $\alpha = \frac{1}{2}(\pi-\phi')$ in the ϕ' integration of (13) yields

$$\int_0^\pi \left(\frac{1}{R^+} - \frac{1}{R^-}\right)d\phi' = \frac{2}{R_1^+}K(u^2) - \frac{2}{R_1^-}K(w^2) \tag{14}$$

where

$$R_1^\pm = \left[(\rho + \rho')^2 + (z \mp z')^2\right]^{1/2} \tag{15}$$

$$u = \frac{2\sqrt{\rho\rho'}}{R_1^+} \tag{16a}$$

$$w = \frac{2\sqrt{\rho\rho'}}{R_1^-} \tag{16b}$$

$$K(m) = \int_0^{\pi/2} \frac{d\alpha}{\sqrt{1 - m\sin^2\alpha}} \tag{17}$$

K(m) is the complete elliptic integral of the first kind [5]. Hence, from (14), (13) can be rewritten as

$$\frac{1}{2\pi^2\varepsilon_0}\int_0^T q(t')\left[\frac{K(u^2)}{R_1^+} - \frac{K(w^2)}{R_1^-}\right]dt' = V \tag{18}$$

Expression (18) is an integral equation for the unknown linear charge density q(t) along the conducting body of revolution. The advantage of (18) over (13) is that there exist polynomial approximations for the elliptic integrals which can be integrated with ease [5]. Once q(t) has been

determined, the capacitance C of the body with respect to ground can be evaluated as

$$C = \frac{Q}{V} = \frac{1}{V} \int_0^T q(t') \, dt' \qquad (19)$$

NUMERICAL FORMULATION

Consider the approximation of the generating curve of the body of revolution as a sequence of N linear segments as shown in Fig. 7. The endpoints of the segments lie on the generating curve and are denoted by $\bar{t}_0, \bar{t}_1, \bar{t}_2, ..., \bar{t}_N$. Each endpoint is described in cylindrical coordinates as $\bar{t}_i = (\bar{\rho}_i, \bar{z}_i)$ i = 0, 1, 2, ..., N. The segment midpoints are given by

$$t_i = \frac{\bar{t}_{i-1} + \bar{t}_i}{2} = \left(\frac{\bar{\rho}_{i-1} + \bar{\rho}_i}{2}, \frac{\bar{z}_{i-1} + \bar{z}_i}{2} \right) = (\rho_i, z_i) \qquad i = 1, 2, ..., N \qquad (20)$$

while the segment lengths are

$$\Delta_i = \left[(\bar{\rho}_i - \bar{\rho}_{i-1})^2 + (\bar{z}_i - \bar{z}_{i-1})^2 \right]^{1/2} \qquad i = 1, 2, ..., N \qquad (21)$$

On segment j ($\bar{t}_{j-1} \le t \le \bar{t}_j$) the following parameterization is valid:

$$z = \bar{z}_{j-1} + (t - \bar{t}_{j-1}) \cos v_j \qquad (22a)$$

$$\rho = \bar{\rho}_{j-1} + (t - \bar{t}_{j-1}) \sin v_j \qquad (22b)$$

where

$$v_j = \tan^{-1} \left(\frac{\bar{\rho}_j - \bar{\rho}_{j-1}}{\bar{z}_j - \bar{z}_{j-1}} \right) \qquad (23)$$

Here, v_j is the angle between the approximate generating curve at $t = t_j$ and the z-axis.

The method of moments [6] may be applied to obtain a numerical solution to the integral equation (18). In this implementation, the linear charge density is approximated as a linear sum of pulses:

$$q(t) \cong \sum_{j=1}^N Q_j P_j(t) \qquad (24)$$

where

7

$$P_j(t) = \begin{cases} 1, & \bar{t}_{j-1} \le t \le \bar{t}_j \\ 0, & \text{elsewhere} \end{cases} \qquad (25)$$

Q_j is the linear charge density at the center of the jth segment $(t = t_j)$. Fig. 8 gives a depiction of the pulse approximation of q(t). The substitution of (24) and (25) into (18) followed by an enforcement of the resulting equation at the center of each segment $(t = t_i, i = 1, 2, ..., N)$ yields a linear system of N equations in the N unknown coefficients Q_j:

$$\sum_{j=1}^{N} Z_{ij} Q_j = V_i \qquad i = 1, 2, ..., N \qquad (26)$$

where

$$V_i = 2\pi^2 \varepsilon_o V \qquad (27)$$

$$Z_{ij} = \int_0^{\Delta_j} \left[\frac{K(u_{ij}^2)}{R_{ij}^+} - \frac{K(w_{ij}^2)}{R_{ij}^-} \right] d\tau' \qquad (28)$$

$$R_{ij}^{\pm} = \left[(\rho_i + \bar{\rho}_{j-1} + \tau' \sin v_j)^2 + (z_i \mp \bar{z}_{j-1} - \tau' \cos v_j)^2 \right]^{1/2} \qquad (29)$$

$$u_{ij} = \frac{2\left[\rho_i \left(\bar{\rho}_{j-1} + \tau' \sin v_j \right) \right]^{1/2}}{R_{ij}^+} \qquad (30a)$$

$$w_{ij} = \frac{2\left[\rho_i \left(\bar{\rho}_{j-1} + \tau' \sin v_j \right) \right]^{1/2}}{R_{ij}^-} \qquad (30b)$$

The integral in (28) was obtained following the change of variables $\tau' = t' - \bar{t}_{j-1}$. In (28), the first term of the integrand possesses a logarithmic singularity when the observation point is within the source region $(i = j)$. From Appendix A,

$$\frac{K(u^2)}{R_1^+} \xrightarrow[t' \to t]{} \frac{1}{2\rho} \left[\ln(4) + \ln(2\rho) - \ln|t - t'| \right] \qquad (31)$$

Since only the last term in (31) is singular, we may subtract it from the integrand and add its analytically evaluated integral. After an appropiate change of variables, we have from (28) and (31),

$$
Z_{ii} = \int_0^{\Delta_i} \left[\frac{K(u_{ii}^2)}{R_{ii}^+} - \frac{K(w_{ii}^2)}{R_{ii}^-} + \frac{1}{2\rho_i} \ln\left| \frac{\Delta_i}{2} - \tau' \right| \right] d\tau' - \frac{1}{2\rho_i} \int_0^{\Delta_i} \ln\left| \frac{\Delta_i}{2} - \tau' \right| d\tau' \qquad (32)
$$

The second integral in (32) may be evaluated analytically as

$$
\frac{1}{2\rho_i} \int_0^{\Delta_i} \ln\left| \frac{\Delta_i}{2} - \tau' \right| d\tau' = \frac{\Delta_i}{2\rho_i} \left[\ln\left(\frac{\Delta_i}{2}\right) - 1 \right] \qquad (33)
$$

The substitution of (33) into (32) gives

$$
Z_{ii} = \int_0^{\Delta_i} \left[\frac{K(u_{ii}^2)}{R_{ii}^+} - \frac{K(w_{ii}^2)}{R_{ii}^-} + \frac{1}{2\rho_i} \ln\left| \frac{\Delta_i}{2} - \tau' \right| \right] d\tau' + \frac{\Delta_i}{2\rho_i} \left[1 - \ln\left(\frac{\Delta_i}{2}\right) \right] \qquad (34)
$$

The representation of Z_{ii} as given by (34) can be integrated numerically.

The linear system of equations (26) may be written in matrix form as follows:

$$
[Z][Q] = [V] \qquad (35)
$$

where $[Z]$ is an N x N coefficient matrix with elements given by (28) and (34) while $[V]$ is the excitation vector with elements given by (27). The unknown charge density vector $[Q] = [Q_1, Q_2, ..., Q_N]^T$ is determined by matrix inversion. An explanation and listing of a FORTRAN language computer program based on the method of moments solution of (18) as described in this section is given in Appendix B.

EXPERIMENTAL SETUP

The numerical algorithm was tested by comparing its results with the measured capacitances of several hollow cylinders at varying distances above the ground plane. Various tubes were

constructed with heights varying from 1 in. to 7 in. and diameters ranging from 3.5 in. to 8.2 in. The capacitances were measured at 100 kHz using a low frequency network analyzer. The ground plane used in this investigation was a 3 ft diameter sheet of 1/4 in. thick steel. These dimensions were found to adequately approximate an infinite ground plane. The tubes were constructed by attaching thin copper tape around PVC pipes of various diameters. A small piece of wire was soldered to the outside of each tube for connection of the network analyzer probe. The distance above the ground plane was varied by placing the tube on top of several small wooden blocks of different thicknesses. The entire measurement setup was placed in a shielded room.

The tubes were also measured with a top load. The top load consisted of an 8 1/4 in. diameter flat disk of copper tape attached to a cardboard backing that was soldered to the tube under study. The measurement repeatability was found to be approximately ±.75 pF for the unloaded tubes and ±1.5 pF for the top-loaded tubes.

RESULTS

Consider a highly conducting tube of length h, radius a, and separated by a distance s above a perfectly conducting ground plane as illustrated in Fig. 9(a). Fig. 10 shows the normalized linear charge density $q(t)/\varepsilon_0 V$ of a tube of length h = 6 in. and diameter 2a = 3.5 in. plotted as a function of axial distance t along the tube for various separations above the ground plane. The curves show a charge singularity at each end of the tube as predicted from theory [7]. For large separations above the ground plane, the charge distribution is symmetric about the midpoint of the tube. As the tube separation above the ground plane becomes small, the charge symmetry disappears with more charge accumulating on the ground plane side of the tube.

Fig. 11 shows a comparison of the computed and measured capacitances of several 6 in. long conducting tubes of different radii plotted as a function of separation above the ground plane. The curves show that the capacitance decreases with separation from the ground plane and increases for larger radii. The data indicate that the measured and computed capacitances agree to within 1 pF for most separations, an excellent correspondence considering the margin for error in the

measurements. A similar comparison of the computed and measured capacitances of several 3 in. long tubes given in Fig. 12 also shows an agreement to within 1 pF. Comparisons for tubes of other heights produced similar results, verifying the accuracy of the body of revolution algorithm.

Appendix C gives an approximate formula (C – 3) for half of the capacitance of an electrically small tubular monopole above a perfectly conducting ground plane. This formula is a modified expression for the capacitance of a coplanar stripline. The advantage of this formula over the moment-method solution is that its evaluation involves only the computation of elliptic integrals of the first kind for which simple polynomial approximations exist [5]. A comparison of the approximate formula with the integral equation solution and measured data for the capacitances of several 5 in. long conducting tubes is given in Fig. 13. The curves show a close agreement with both the measured and integral equation data, indicating the adequacy of the modified coplanar stripline formula for computing the capacitance of an electrically small monopole or dipole antenna. For additional results, the reader is referred to [8].

Consider the top-loaded tube shown in Fig. 9(b). It consists of a highly conducting thin disk of radius b that is attached to the tube in Fig. 9(a). Since the geometry of the top-loaded tube is not tractable using the body of revolution algorithm described in the previous section, the top load and the tube had to be analyzed as two coupled bodies of revolution. The specifics of a revised algorithm to analyze this structure will not be given in this report as it is a direct extension of the previously described body of revolution algorithm.

Fig. 14 shows a comparison of the computed and measured capacitances of several top-loaded conducting tubes with h = 6 in. and 2b = 8.25 in. of different radii plotted as a function of separation above the ground plane. The data show the same behavior as the unloaded tubes in Fig. 11 except that the capacitances are larger. The data also show more deviation between the measured and computed results. This is expected since the measurement repeatability is worse in this case. A similar comparison of the computed and measured capacitances of several top-loaded tubes with h = 3 in. and 2b = 8.25 in. is given in Fig. 15. Comparisons for top-loaded tubes of other heights with 2b = 8.25 in. produced similar results, further verifying the accuracy of the revised body of

revolution algorithm.

The body of revolution algorithm was also applied to compute the static charge distribution and capacitance of a conical antenna over a conducting ground plane. Our computed data compare well with Wilton's computed data [9] for various conical antennas both with and without a top load.

When the body of revolution described in Fig. 6 is used as an antenna, it must be connected to a receiver located below the ground plane. Therefore, the portion of the connecting wire above the ground plane and the body of revolution form an antenna which acts as a monopole. Since the connecting wire is at the same potential as the body of revolution, the antenna capacitance is the sum of the wire and body capacitances. If the connecting wire is very thin such that it carries a negligible charge as compared with the total charge on the body, its capacitance may be ignored. In this report, the capacitance of the connecting wire will be neglected.

EFFECTIVE HEIGHT

The effective height h_{eff} of a linearly polarized antenna receiving a plane wave from a given direction is the ratio of the magnitude of the open circuit voltage developed at the terminals of the antenna to the magnitude of the electric field strength in the direction of the antenna polarization [10]. This definition has been applied in (1). Alternatively, the effective height is the length of a thin straight conductor oriented perpendicular to the given direction and parallel to the antenna polarization, having a uniform current equal to that at the antenna terminals and producing the same far-field strength as the antenna in that direction [10]. The application of this latter definition to the body of revolution in Fig. 6 yields

$$h_{eff} = \frac{1}{I(0)} \int_0^T I(t) \cos v(t) \, dt \qquad (36)$$

where T is the arc length along the generating curve of the antenna, v(t) is the angle between the tangent to the generating curve and the z-axis, I(t) is the current along the antenna, and I(0) is the current at the antenna terminals. It is assumed that the body is separated by an infinitesimal

distance from the ground plane.

An expression for the effective height of a body of revolution may be obtained in terms of the charge distribution. The application of the method of moments formulation described in the previous section to the effective height formula (36) gives

$$h_{eff} = \frac{1}{I(0)} \sum_{i=1}^{N} \cos v_i \int_{\bar{t}_{i-1}}^{\bar{t}_i} I(t)\, dt \qquad (37)$$

From the continuity equation,

$$I'(t) = -j\omega q(t) \qquad (38)$$

The integration of (38) over the entire antenna yields

$$I(T) - I(0) = -j\omega \int_0^T q(t)\, dt$$

Since $I(T) = 0$,

$$I(0) = j\omega \int_0^T q(t)\, dt = j\omega \sum_{i=1}^{N} Q_i \Delta_i \qquad (39)$$

where $Q_i \Delta_i$ is the total charge on segment i. The application of (38) to the integral in (37) gives

$$\int_{\bar{t}_{i-1}}^{\bar{t}_i} I(t)\, dt = \bar{t}_i I(\bar{t}_i) - \bar{t}_{i-1} I(\bar{t}_{i-1}) + \frac{j\omega}{2} Q_i \Delta_i \left(\bar{t}_{i-1} + \bar{t}_i\right) \qquad (40)$$

Upon repeated application of (38),

$$I(\bar{t}_i) = j\omega \sum_{j=i+1}^{N} Q_j \Delta_j \qquad (41)$$

The substitution of (41) into (40) yields

$$\int_{\bar{t}_{i-1}}^{\bar{t}_i} I(t)\, dt = j\omega \Delta_i \sum_{j=i}^{N} \gamma_{ij} Q_j \Delta_j \qquad (42)$$

where

13

$$\gamma_{ij} = \begin{cases} 1/2, & i=j \\ 1, & \text{otherwise} \end{cases} \tag{43}$$

The substitution of (39) and (42) into (37) gives

$$h_{eff} = \frac{\displaystyle\sum_{i=1}^{N} \Delta_i \cos v_i \sum_{j=i}^{N} \gamma_{ij} Q_j \Delta_j}{\displaystyle\sum_{i=1}^{N} Q_i \Delta_i}$$

$$= \frac{\displaystyle\sum_{i=1}^{N} Q_i \Delta_i \sum_{j=1}^{i} \gamma_{ij} \Delta_j \cos v_j}{\displaystyle\sum_{i=1}^{N} Q_i \Delta_i} = \frac{\displaystyle\sum_{i=1}^{N} Q_i \Delta_i \left(z_i - \bar{z}_0\right)}{\displaystyle\sum_{i=1}^{N} Q_i \Delta_i} \tag{44}$$

Equation (44) indicates that the effective height of an electrically small body of revolution is actually the axial height of the center of charge. The above expression also shows the importance of capacitive loading at the top of the antenna since it raises the center of charge and thus increases the effective height of the antenna. A good discussion of the effective height of electrically small linear antennas is given by Schelkunoff and Friis [1].

The above formulation applies to a body of revolution that is separated by an infinitesimal distance from the ground plane. If the body is separated by a finite distance s (= $\bar{z}_0$) above the ground plane and connected to a receiver (located below the ground plane) by a thin wire, the effective height formula (36) must be modified. If the connecting wire is very thin such that it carries a negligible charge as compared with the total charge on the body of revolution, the center of charge of the antenna (connecting wire + body of revolution) is approximately the same as that of the body. Hence, the effective height formula (36) becomes

$$h_{eff} = s + \frac{1}{I(0)} \int_0^T I(t) \cos v(t) \, dt \tag{45}$$

while the numerical formula (44) is

$$h_{eff} = s + \frac{\sum\limits_{i=1}^{N} Q_i \Delta_i \left(z_i - s\right)}{\sum\limits_{i=1}^{N} Q_i \Delta_i} \tag{46}$$

EXAMPLES

Fig. 16 shows the effective height plotted as a function of diameter for a conducting tube of height h = 6 in. and separated by 0.1 in. above a ground plane. In this and all remaining plots, it is assumed that the antenna is connected to a receiver (located below the ground plane) by an infinitesimally thin wire so that (45) and (46) are valid. As the tube diameter approaches zero, the charge distribution becomes nearly symmetrical about its center, resulting in an effective height of almost 3.1 in. As the tube diameter increases, the added capacitive coupling from the lower end of the tube to ground causes the effective height to decrease.

Fig. 17 illustrates a conducting tube of height h and diameter 2a that is top loaded with a thin annular disk of inner diameter 2a and outer diameter 2b. The tube is separated by a short distance s above a ground plane. Fig. 18 shows the effective height of a top-loaded tube with h = 6 in., 2a = 0.5 in., and s = 0.1 in. that is plotted as a function of the top load outer diameter. The curve illustrates the improvement in effective height resulting from an increase in the size of the top load.

Consider the truncated cone described in Fig. 19. It consists of a section of hollow cone with axial length h, lower diameter d_i, and upper diameter d_f. The cone is separated by a small gap s above a perfectly conducting ground plane and connected to a receiver below the ground plane by an infinitesimally thin wire. Fig. 20 shows the effective height of a truncated cone with h = 6 in., d_f = 5 in., and s = 0.1 in. that is plotted as a function of the lower diameter d_i. A narrower initial diameter reduces the capacitive coupling from the lower end of the cone to ground, thereby raising the center of charge of the antenna. Consequently, the curve shows that the effective height increases with a narrower initial diameter. However, as will be shown in the next section, this

increase in effective height is attained at the expense of a decrease in capacitance.

DETERMINATION OF AN OPTIMUM ANTENNA

During this investigation, certain space restrictions for the Loran-C antenna were set. It was decided that the antenna must fit within a cylinder of height 4.25 in. and diameter 5 in., where the bottom of the cylinder is coincident with the sea water line. The Loran antenna may be top loaded but must allow for a feed cable to pass through its middle for connection to a GPS antenna. Thus, it was decided to reserve a cylinder of diameter 0.5 in. in the middle of the Loran antenna for the passage of the GPS antenna feed. The space restrictions for the Loran-C antenna are illustrated in Fig. 21.

Measurements of the FET amplifier were made at 100 kHz to determine the equivalent noise sources E_n and I_n as defined in Fig. 4. The results of these measurements indicated that for antenna capacitances below 100 pF the amplifier is current noise limited; i.e., the noise produced due to I_n is much greater than that due to E_n. Therefore, in any calculations of the amplifier noise field as determined by (7), the contribution due to E_n will be neglected. The measurements, based on a 100 Hz bandwidth signal with a 100 kHz carrier frequency, indicate that I_n is approximately 2 pA.

In this section, an optimum monopole antenna configuration will be determined. The optimum antenna will be one that fits within the space restrictions as described in Fig. 21 and will result in a minimum amplifier noise field as computed by (7). The antenna geometries to be considered are cylinders and truncated cones. Each structure will be studied both with and without a top load.

CYLINDER

Consider a tubular monopole as described in Fig 9(a) with h = 4.15 in. and s = 0.1 in. The antenna capacitance, effective height, and amplifier noise field are plotted as functions of the tube diameter in Figs. 22a, 22b, and 22c, respectively. The curves show that the antenna capacitance is

a monotonically increasing function of the tube diameter while the effective height is a decreasing function. The amplifier noise field E^{amp} as computed from (7) is inversely proportional to the product of the effective height and the antenna capacitance for a current noise limited system. Fig. 22c shows that E^{amp} is a monotonically decreasing function of the tube diameter. Therefore, the change in capacitance due to a variation in the tube diameter overrides the opposite change in the effective height. For example, a tubular monopole with 2a = 0.5 in. yields C_a = 3.52 pf, h_{eff} = 1.80 in., and E^{amp} = 19.8 µV/m while a tube with 2a = 5 in. gives C_a = 22.4 pf, h_{eff} = 1.32 in., and E^{amp} = 4.24 µV/m. Upon increasing the tube diameter from 0.5 in. to 5 in., the capacitance increases by more than a factor of 6 while the effective height decreases by less than 1.5. Consequently, the amplifier noise field decreases by more than a factor of 4.5, corresponding to an improvement of 13.4 dB. Thus, the data in Fig. 22c indicate that the optimum tubular monopole is one with the maximum allowable diameter (2a = 5 in.).

If the tube is top loaded with a conducting annular disk of inner diameter 0.5 in. and outer diameter 5 in. as described in Fig. 17, some improvement in performance can be obtained. For example, a top-loaded tube with h = 4.15 in., s = 0.1 in., and 2a = 0.5 in. results in C_a = 7.36 pf, h_{eff} = 3.23 in., and E^{amp} = 5.27 µV/m while a tube with 2a = 5 in. gives C_a = 22.7 pf, h_{eff} = 1.39 in., and E^{amp} = 3.96 µV/m. Thus, top loading provides an 11.5 dB decrease in the amplifier noise field for the 0.5 in. diameter tube while only resulting in a 0.59 dB improvement for the 5.0 in diameter tube. However, the larger tube still gives the best performance.

TRUNCATED CONE

Consider the top-loaded truncated cone described in Fig. 23. The antenna capacitance, effective height, and amplifier noise field are plotted as functions of the lower diameter d_i in Figs. 24a, 24b, and 24c, respectively, for the truncated cone both with and without the top load. The curves show that the antenna capacitance increases with d_i while the effective height exhibits the opposite behavior. In addition, Fig. 24c indicates that E^{amp} is a monotonically decreasing function of d_i. Consequently, the increase in capacitance associated with an increase in the lower diameter

overrides the corresponding decrease in the effective height. Therefore, tapering the antenna at the base does not provide an improvement in the overall antenna performance. For example, an unloaded cone with $d_i = 0.5$ in. results in $E^{amp} = 5.02$ μV/m while one with $d_i = 5.0$ in. gives $E^{amp} = 4.24$ μV/m. This increase in the lower diameter only results in a 1.47 dB improvement in the amplifier noise field. Note that a truncated cone with $d_i = d_f$ is just a cylinder. The amplifier noise curves in Fig. 24c show that the cylindrical monopole with $2a = 5$ in. provides a lower amplifier noise field than a truncated cone.

Fig. 24c shows that a top-loaded cone provides a lower amplifier noise field than an unloaded cone. However, this improvement is quite small. For example, a top-loaded truncated cone with $d_i = 0.5$ in. results in only a 0.67 dB improvement over an unloaded one.

FINAL DESIGN

The analysis of the previous section has shown that the optimum Loran-C antenna that fits within the space restrictions described in Fig. 21 is a tubular monopole with the maximum allowable diameter ($2a = 5$ in.). From Figs. 22a–22c, this antenna results in $C_a = 22.4$ pF, $h_{eff} = 1.32$ in., and $E^{amp} = 4.24$ μV/m. Although the analysis showed that a top-loaded tube performs slightly better than an unloaded tube (0.59 dB improvement), the top load was omitted for mechanical reasons.

Fig. 25 gives a schematic view of the Loran-C antenna and amplifier assembly. For mechanical reasons, the antenna and the amplifier were enclosed in a 1/16 in. thick fiberglas tube of 5 in. outer diameter. The antenna was constructed from a 1/16 in. thick aluminum tube that fits tightly against the fiberglas housing. The amplifier was enclosed in a grounded aluminum can of 0.965 in. height and the same diameter as the antenna. The can included a 3/16 in. diameter hole through its middle for passage of the GPS antenna feed cable. The Loran-C antenna and amplifier assembly in Fig. 25 was enclosed in a cylindrical radome made of lexan ($\varepsilon_r \cong 3$) and further surrounded by a floatation collar made of syntactic foam ($\varepsilon_r \cong 1.5$).

Since the amplifier required a larger enclosure than previously anticipated (0.965 in. height instead of 0.75 in.), the antenna height was reduced to 3.785 in. while the fiberglas housing reduced the antenna diameter to approximately 4 7/8 in. Additionally, the tube was separated by 0.25 in. from the ground plane. The recalculation of the parameters for this smaller antenna (h = 3.785 in., 2a = 4.875 in., and s = 0.25 in.) yields C_a = 17.8 pF, h_{eff} = 1.53 in., and E^{amp} = 4.60 μV/m. From the CCIR tables [4], the atmospheric noise (for a 100 Hz bandwith) near the coast of Connecticut ranges from a minimum of 0.94 μV/m during the Winter to a maximum of 21 μV/m during the Summer. Thus, according to these numbers, the Loran antenna/amplifier system is usually atmospheric noise limited.

The effective height of the Loran antenna was measured by comparing the received signal strength from a Loran station with that from a VLF loop antenna of known effective height. Based on this method, the measured effective height was approximately 1 in., smaller than the number predicted. The smaller measured effective height is probably due to the added capacitive loading from the dielectric surrounding the antenna and the finite thickness of the connecting wire. Reception problems occurred when the floatation collar became wet. The measurements were carried out over a salt water pond in Fisher's Island, NY.

SUMMARY AND CONCLUSIONS

This report has provided a systematic theoretical determination of an optimum monopole antenna configuration for Loran-C reception that fits within certain space requirements. The antenna analysis was based on a quasi-static numerical study of a conducting body of revolution above a perfectly conducting ground plane. An optimum antenna is one that results in a minimum amplifier noise field as computed from (7).

An integral part of this study included a determination of the amplifier noise. On account of the small dimensions allotted for the Loran antenna, the antenna capacitance was sufficiently small so that the amplifier was current noise limited (see Fig. 4), resulting in a noise field that is

inversely proportional to the product of the antenna capacitance and effective height. Consequently, the study showed a tradeoff in the effort to obtain both a large antenna capacitance and effective height. For example, a structure which is more tapered at the base yields an increase in effective height at the expense of a loss in capacitance. The analysis showed that the optimum monopole antenna is a hollow cylinder of maximum allowable diameter and a small separation from the ground plane. The analysis also indicated that the addition of a top load provides a small increase in both the antenna capacitance and effective height resulting in an improved performance. However, because of mechanical constraints, it was decided to omit the top load.

Measurements performed on the Loran-C antenna indicate a lower effective height than the predicted value because of the finite thickness of the connecting wire and the added shunt capacitive loading from the dielectric surrounding the antenna. The computer program for the conducting body of revolution assumes an upper-half space consisting of air and does not account for any dielectric loading. The Loran antenna performance degraded significantly when it became wet.

REFERENCES

1. S. A. Schelkunoff and H. T. Friis, *Antennas: Theory and Practice*, Ch. 10, J. Wiley & Sons, New York, NY, 1952.

2. E. C. Jordan and K. G. Balmain, *Electromagnetic Waves and Radiating Systems*, pp. 351-353, Prentice-Hall, Englewood Cliffs, NJ, 1968.

3. C. D. Motchenbacher and F. C. Fitchen, *Low-Noise Electronic Design*, J. Wiley & Sons, New York, NY, 1973.

4. CCIR Report No. 322, *World Distribution and Characteristics of Atmospheric Noise*, International Telecommunication Union, Geneva, 1964.

5. M. Abramowitz and I. A. Stegun, *Handbook of Mathematical Functions*, Ch. 17, National Bureau of Standards, AMS 55, U. S. Dept. of Commerce, Washington, D.C., 1964.

6. R. F. Harrington, *Field Computation by Moment Methods*, R. E. Krieger Publishing Co., Malabar, FL, 1982.

7. J. D. Jackson, *Classical Electrodynamics*, Second Edition, pp. 75-78, J. Wiley & Sons, New York, NY, 1975.

8. J. P. Casey and R. Bansal, "Capacitance of a Small Tubular Antenna", *Electronics Letters*, Vol. 24, pp. 1021-1022, 4th August 1988.

9. D. R. Wilton, "Static Analysis of Conical Antenna Over a Ground Plane", University of Mississippi, AFOSR-TR-76-1078, Air Force Office of Scientific Research, Bolling AFB, Washington, D.C., August, 1976.

10. IEEE, "IEEE Standard Definitions of Terms for Antennas", IEEE Std 145-1983, *IEEE Transactions on Antennas and Propagation*, Vol. AP-31, Part II, November 1983.

11. A. W. Glisson and D. R. Wilton, "Simple and Efficient Numerical Techniques for Treating Bodies of Revolution", University of Mississippi, RADC-TR-79-22, Rome Air Development Center, Griffiss AFB, NY, March 1979.

12. A. Ralston and P. Rabinowitz, *A First Course in Numerical Analysis*, Second Edition, pp. 421-422, McGraw-Hill, New York, NY, 1978.

13. G. J. Burke and A. J. Poggio, "Numerical Electromagnetics Code (NEC) - Method of Moments, Parts I, II, and III", Technical Document 116, Naval Ocean Systems Center, San Diego, CA, January 1981.

14. V. F. Hanna, "Finite Boundary Corrections to Coplanar Stripline Analysis", *Electronics Letters*, **16**, pp. 604-606, 17th July 1980.
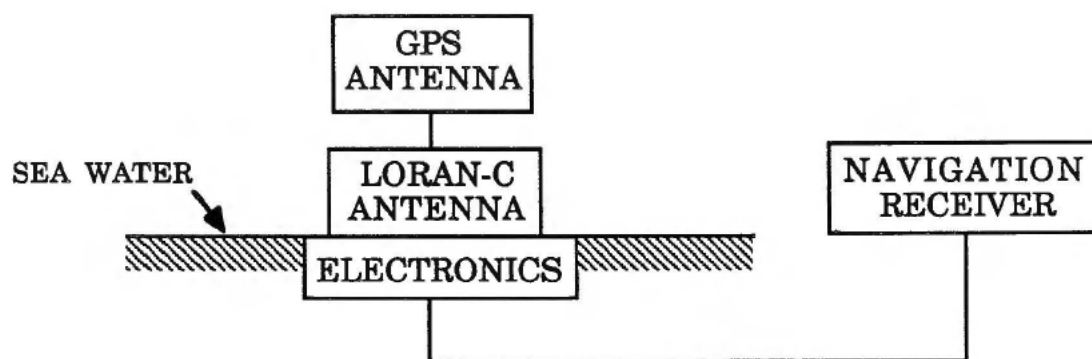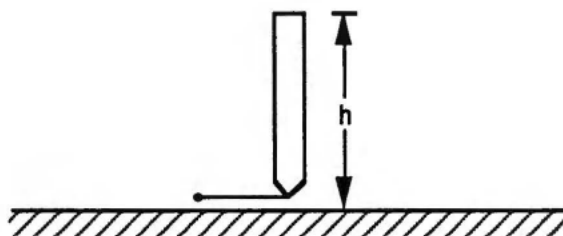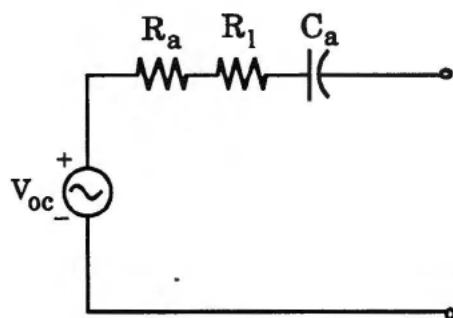
Figure 1   Loran-C/GPS integrated antenna system.
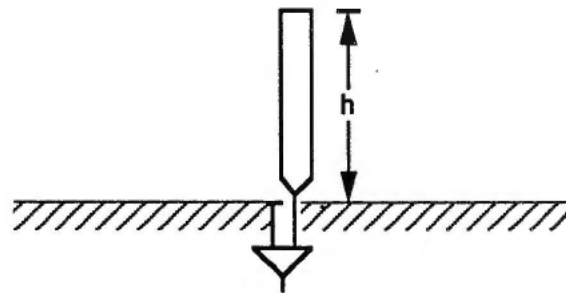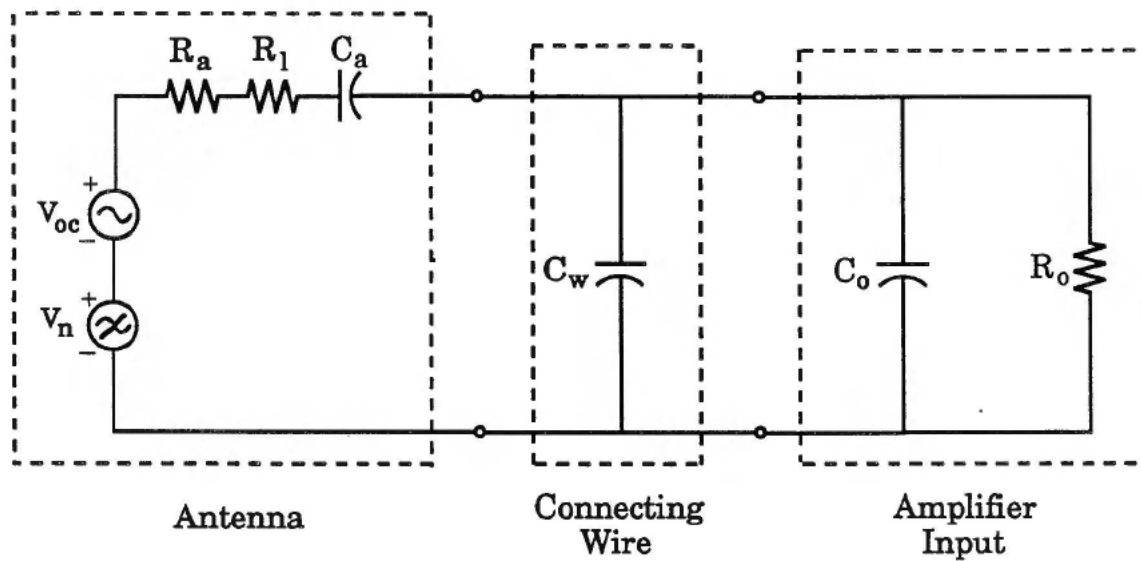
(a)

(b)

Figure 2.   (a) Monopole antenna above a ground plane.
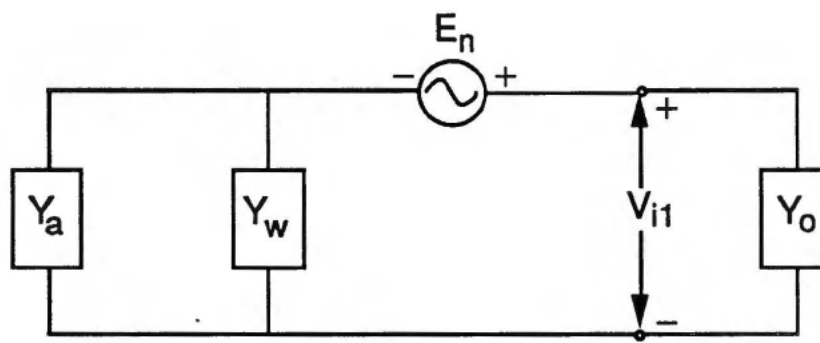   (b) Thevenin equivalent circuit in the receiving mode.
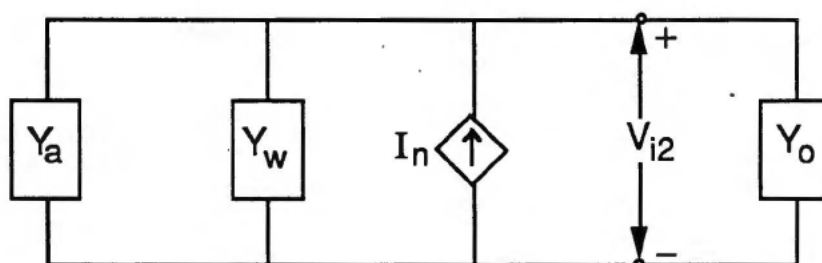
(a)

(b)

Figure 3. (a) Monopole antenna connected to an FET amplifier.
(b) Equivalent circuit.

(a)

(b)

Figure 4.   Amplifier noise model.
        (a) Input noise voltage E_n of the amplifier.
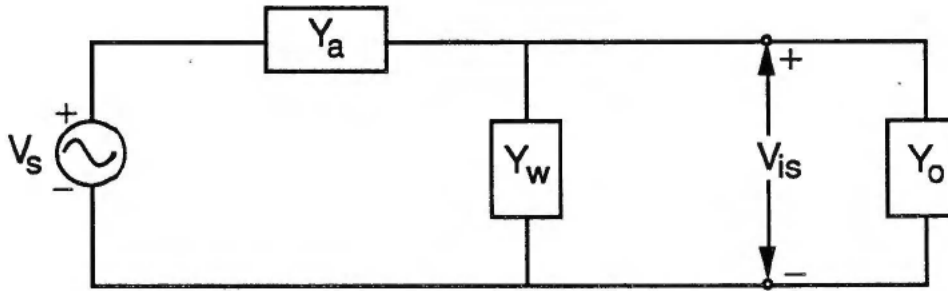   (b) Input noise current I_n of the amplifier.

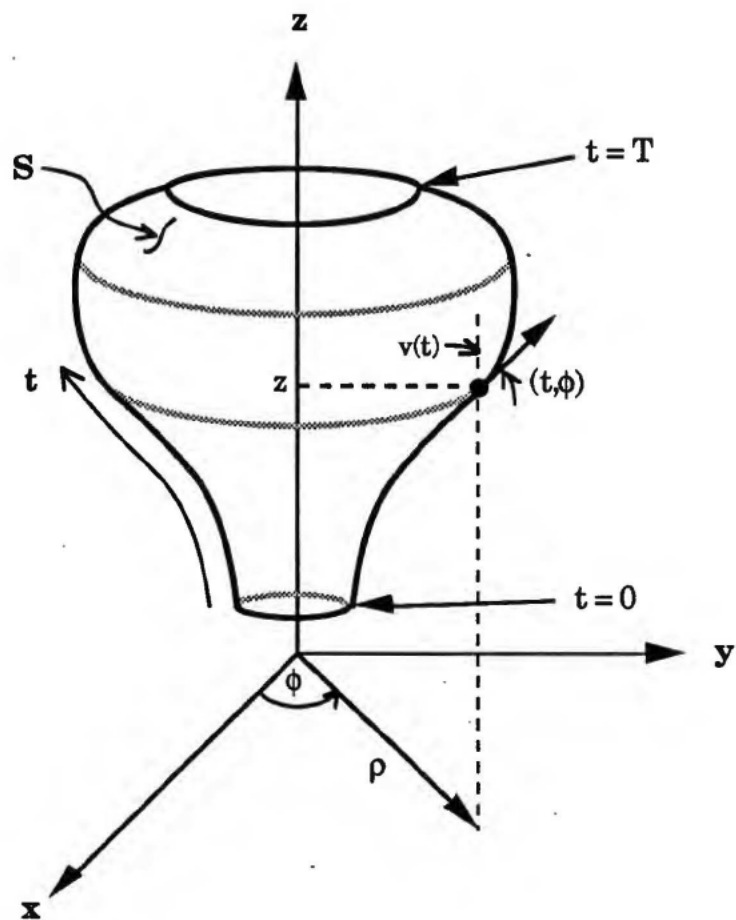Figure 5.   Equivalent circuit for determination of the voltage transfer function.

Figure 6.   Body of revolution and coordinate system.
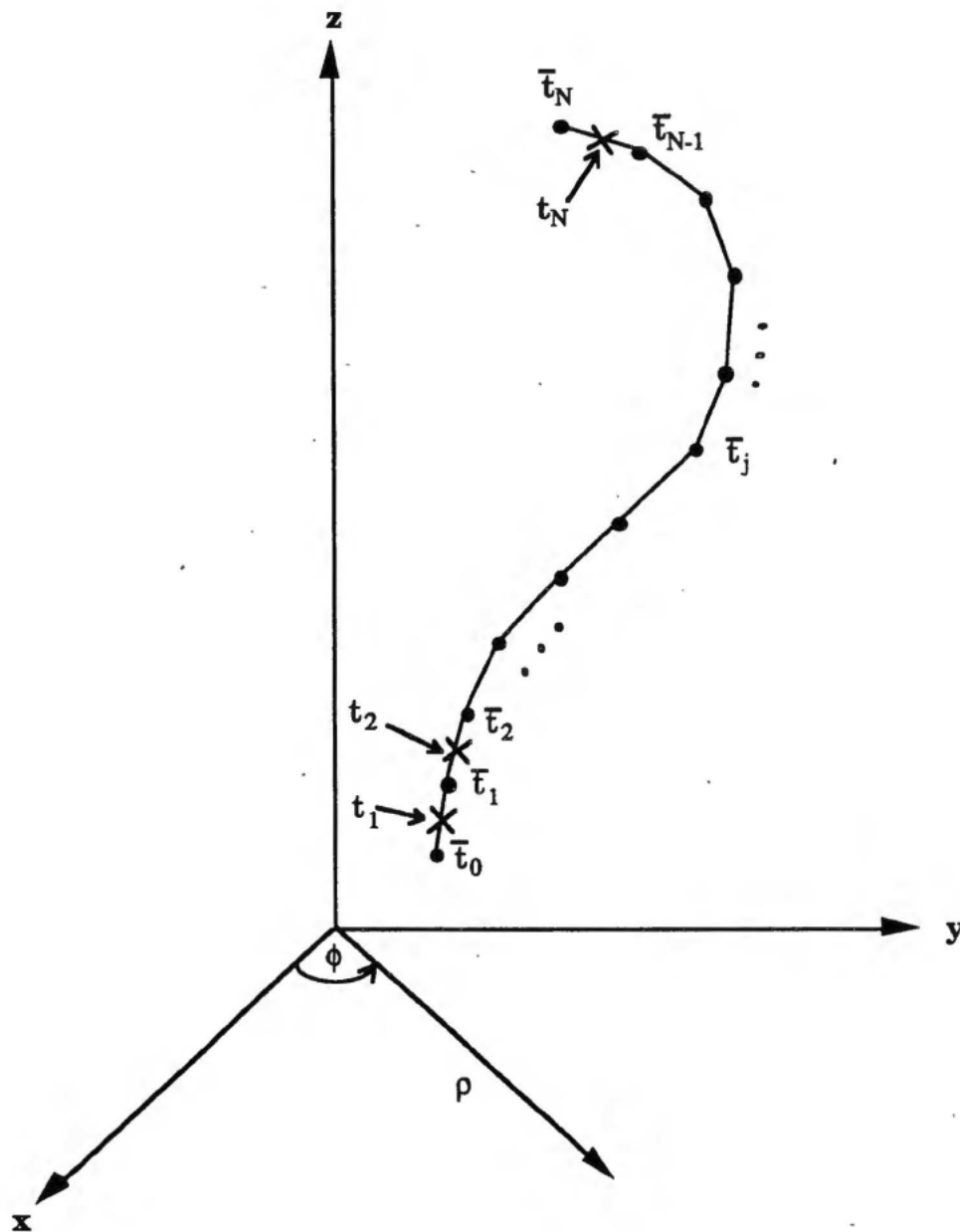
Figure 7. Approximation of the generating curve as linear segments for the body of revolution in Fig. 6.
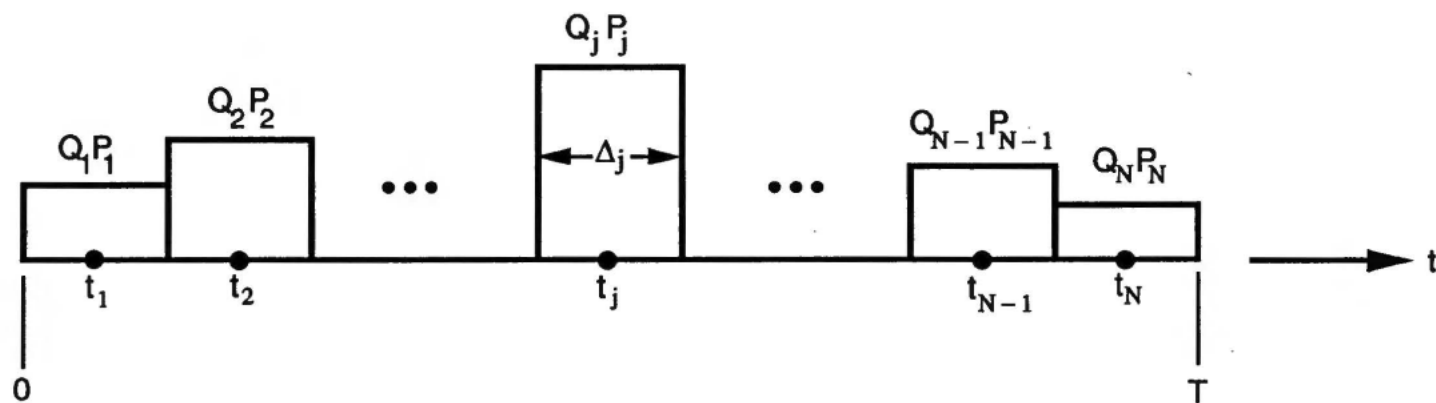
Figure 8.   Pulse expansion scheme for the linear charge density q(t).
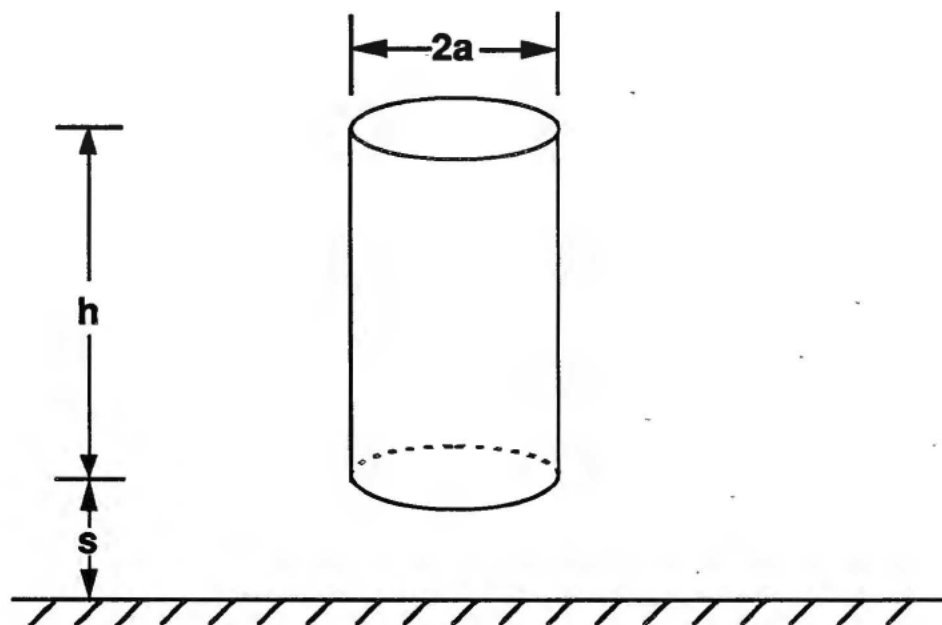
(a)
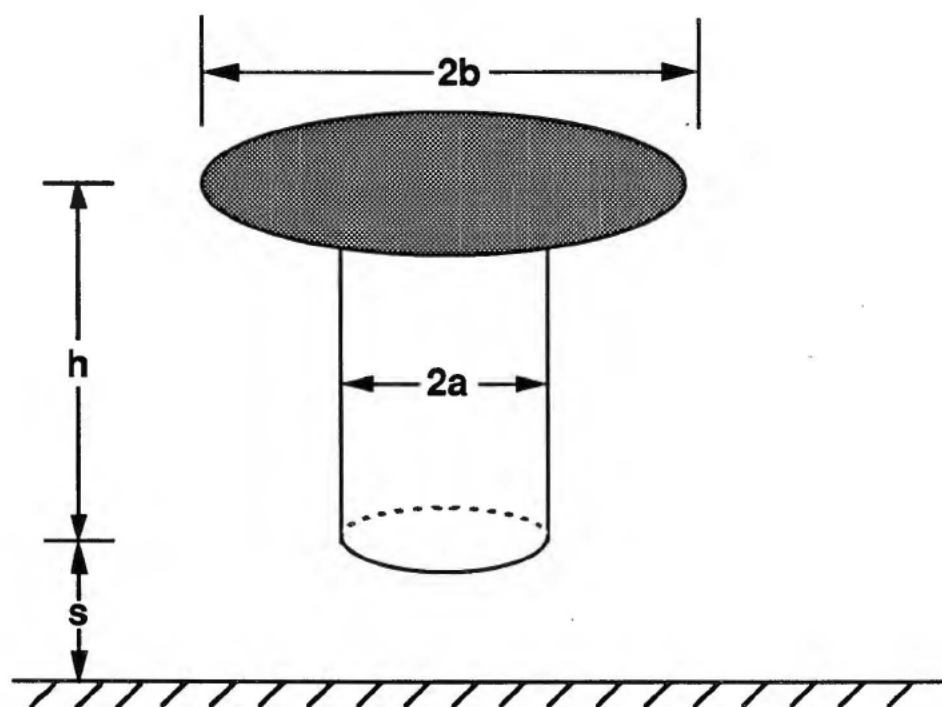
(b)

Figure 9.   Conducting tube above a ground plane.
(a) without top load
(b) with top load
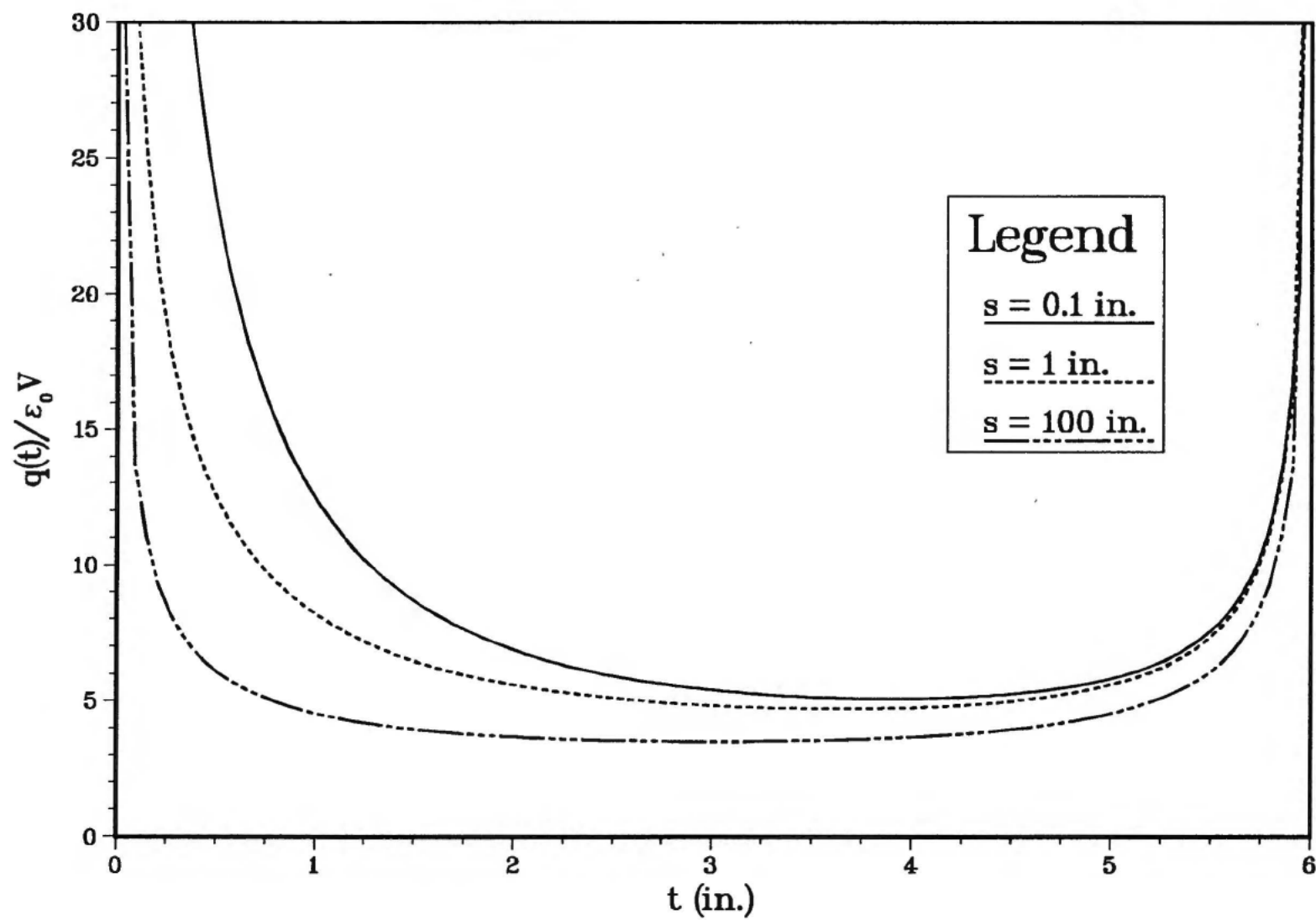
Figure 10. Normalized linear charge density along a conducting tube (h = 6 in., 2a = 3.5 in.) for various separations above a ground plane.
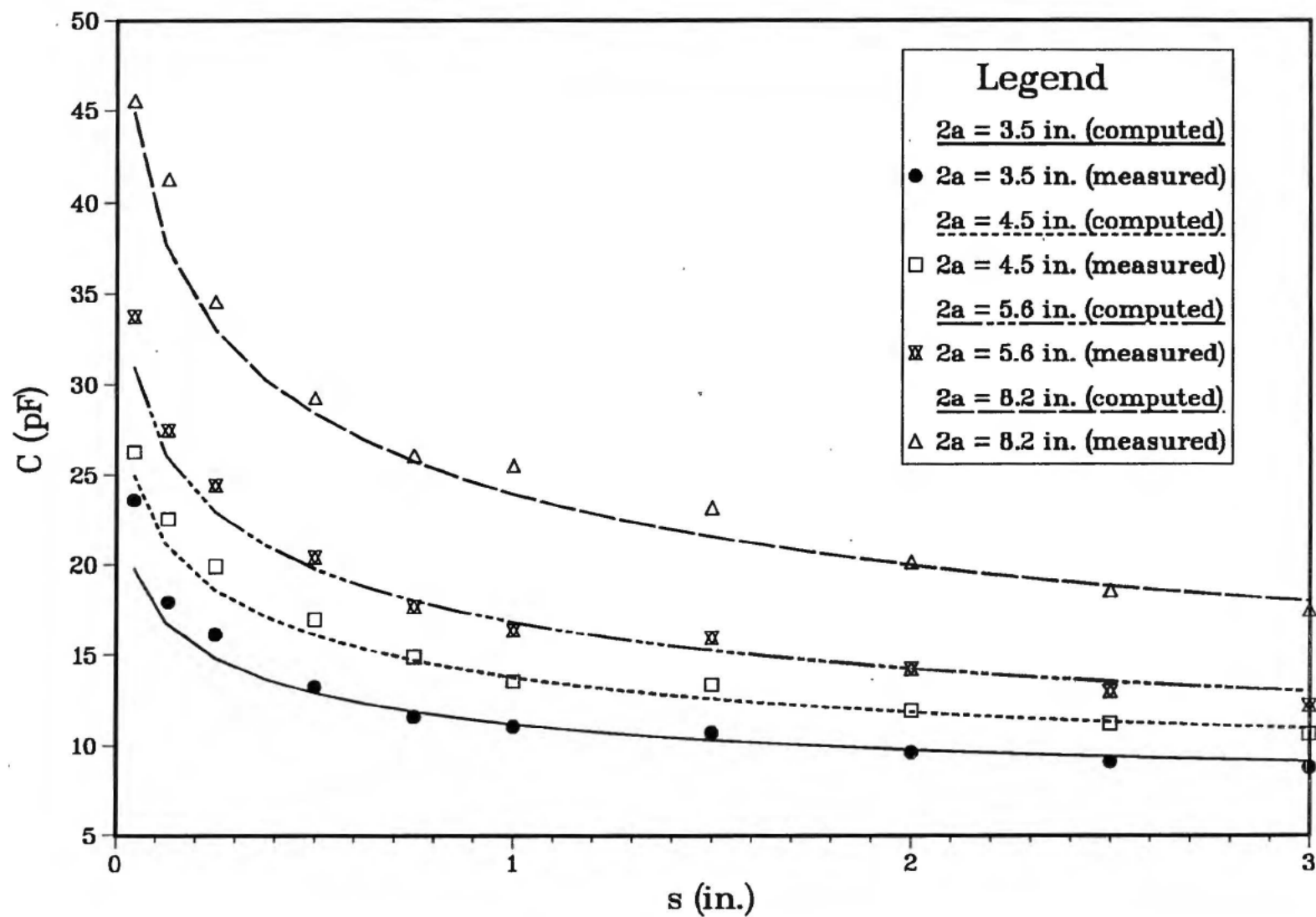
Figure 11. Capacitances of several conducting tubes (h = 6 in.) of different radii as a function of separation above a ground plane.
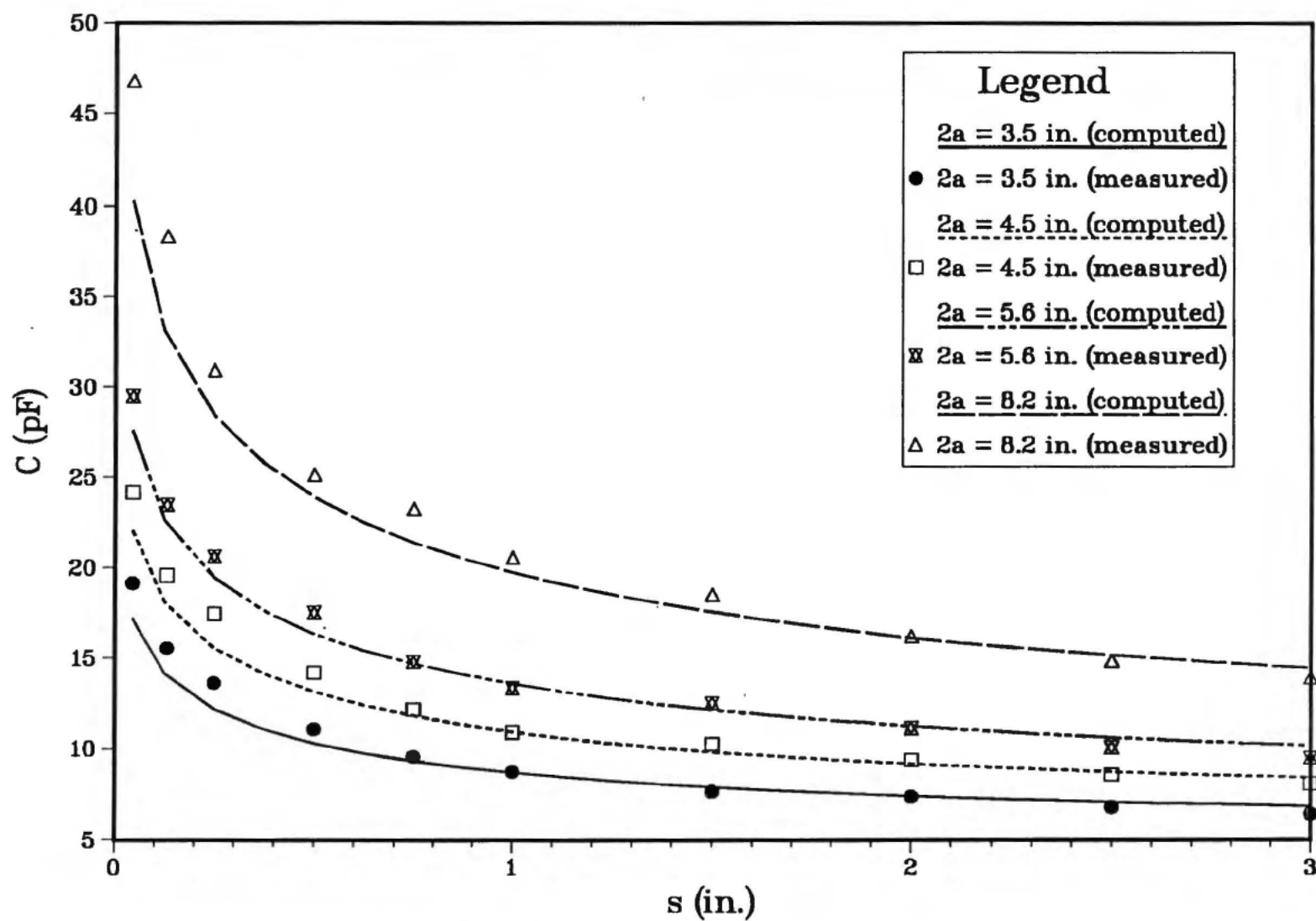
Figure 12. Capacitances of several conducting tubes (h = 3 in.) of different radii as a function of separation above a ground plane.
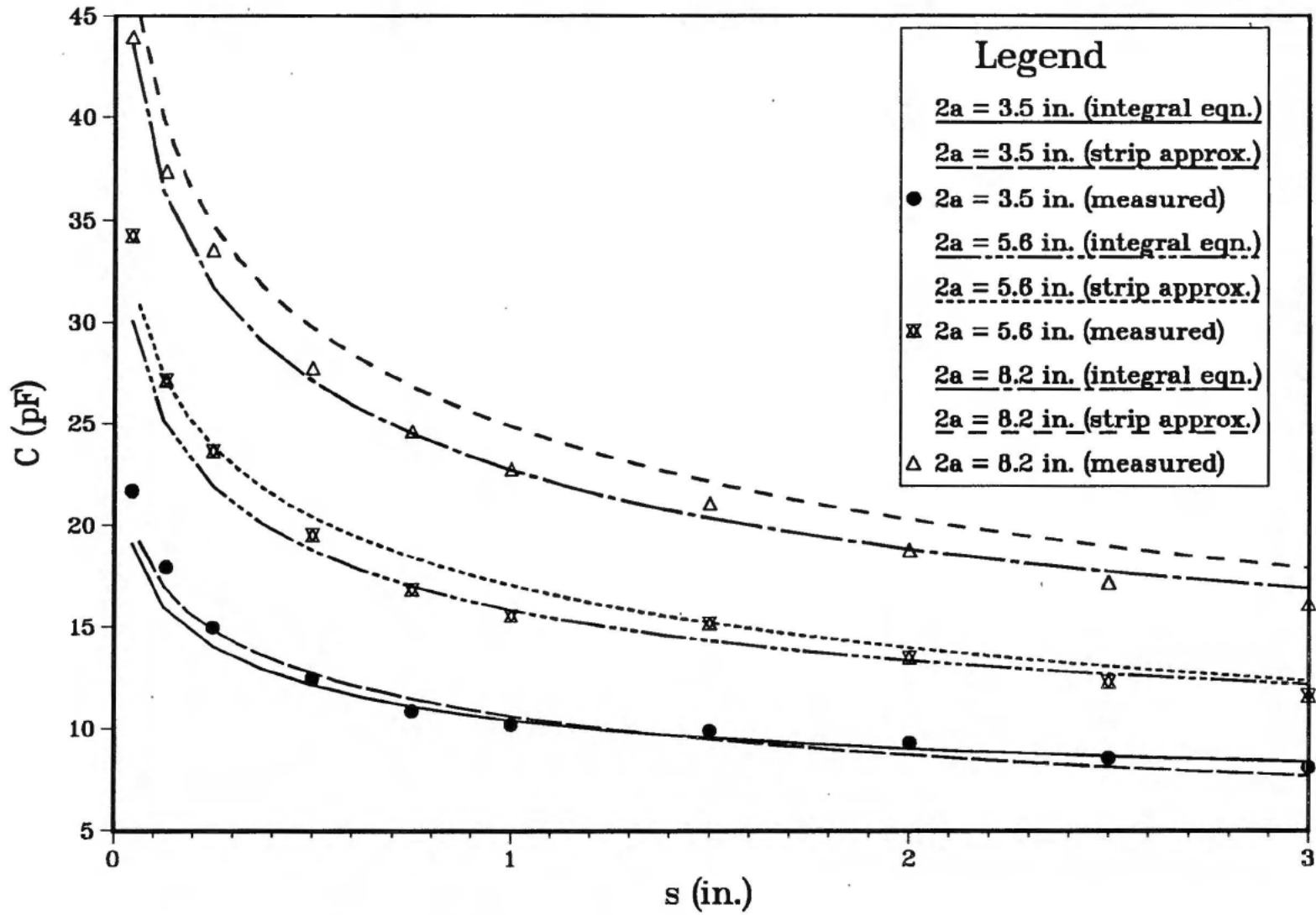
Figure 13. Capacitances of several conducting tubes (h = 5 in.) of different radii as determined by various methods.
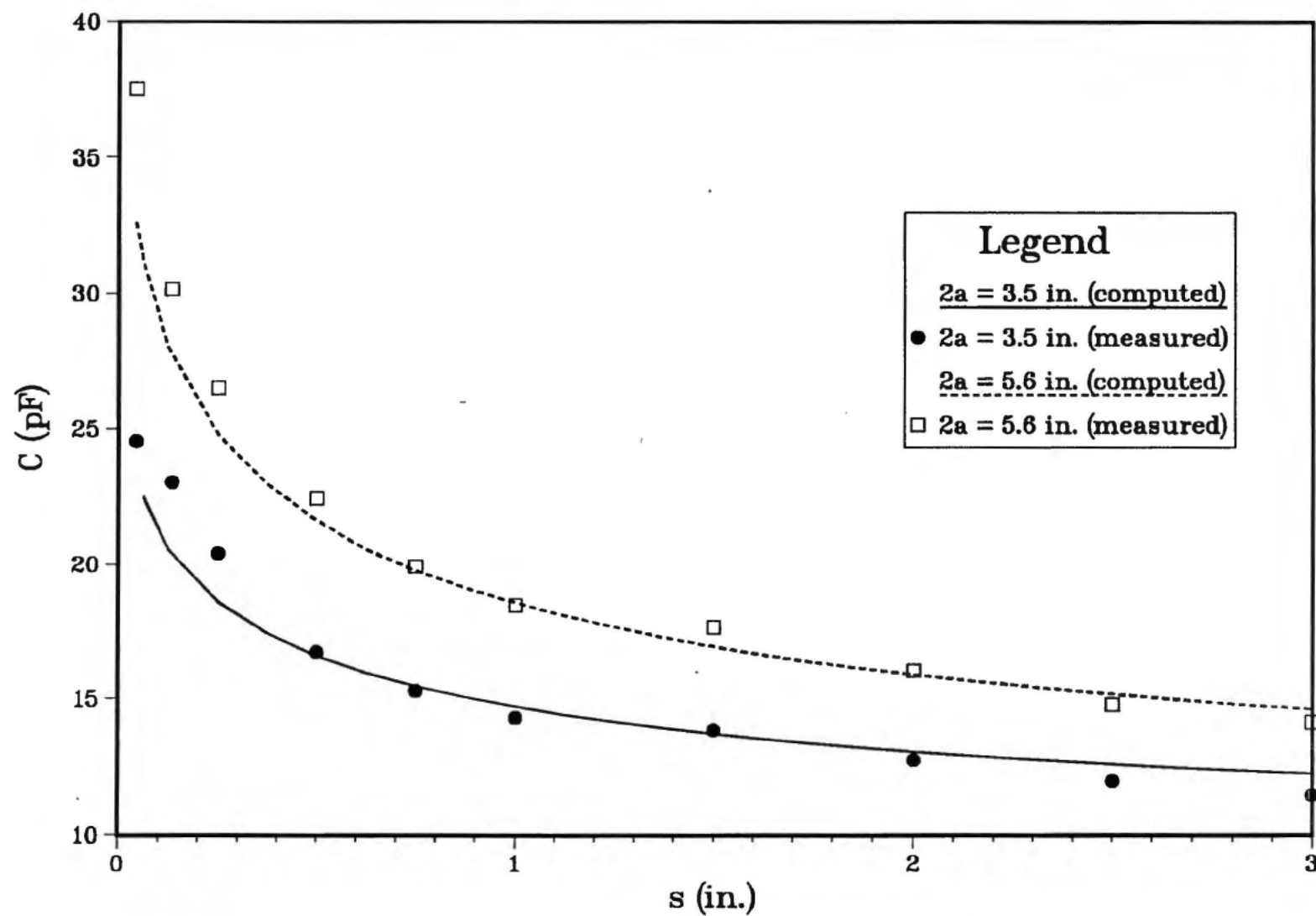
Figure 14. Capacitances of several top-loaded conducting tubes (h = 6 in., 2b = 8.25 in.) of different radii as a function of separation above a ground plane.
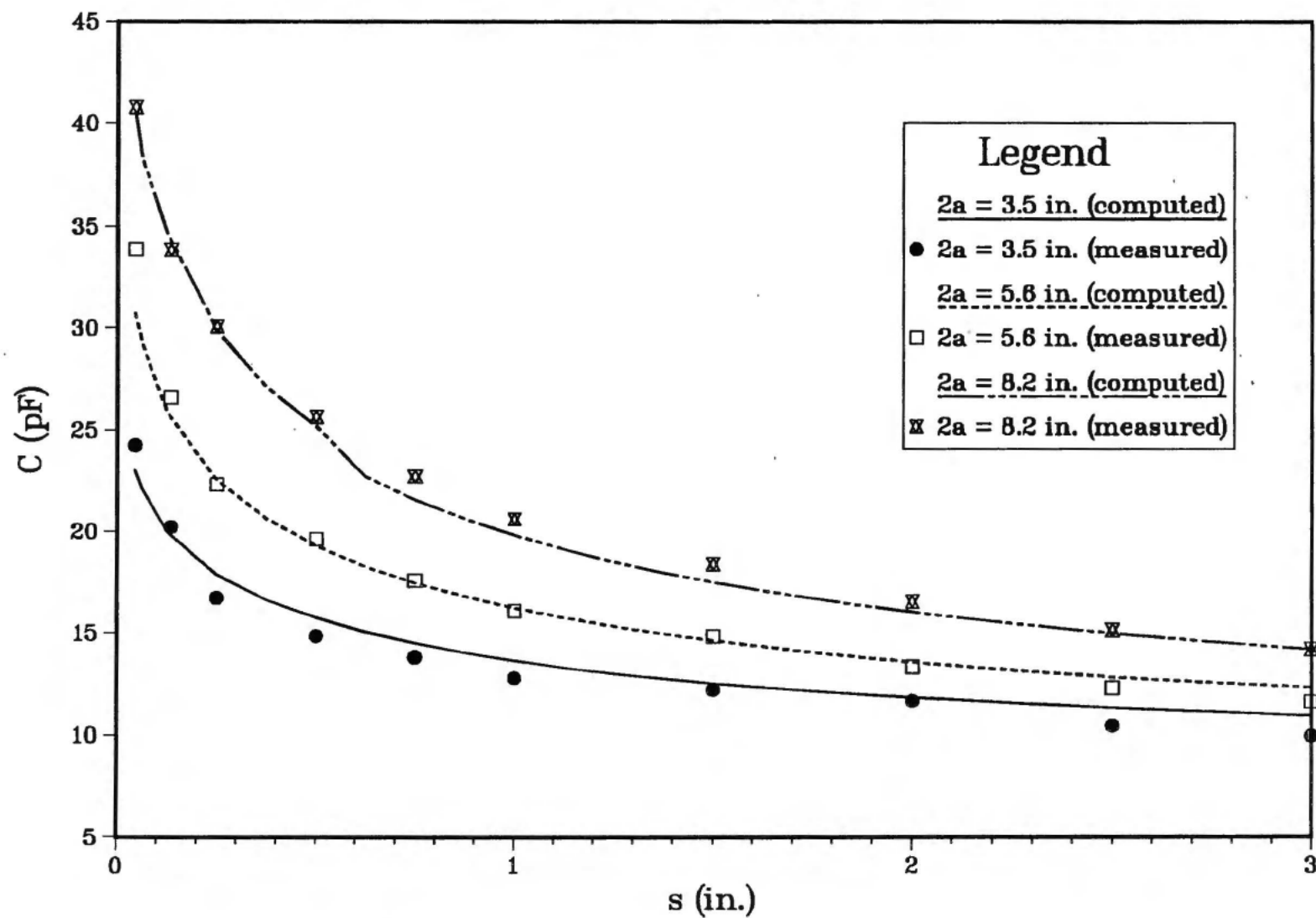
Figure 15.   Capacitances of several top-loaded conducting tubes (h = 3 in., 2b = 8.25 in.) of different radii as a function of separation above a ground plane.
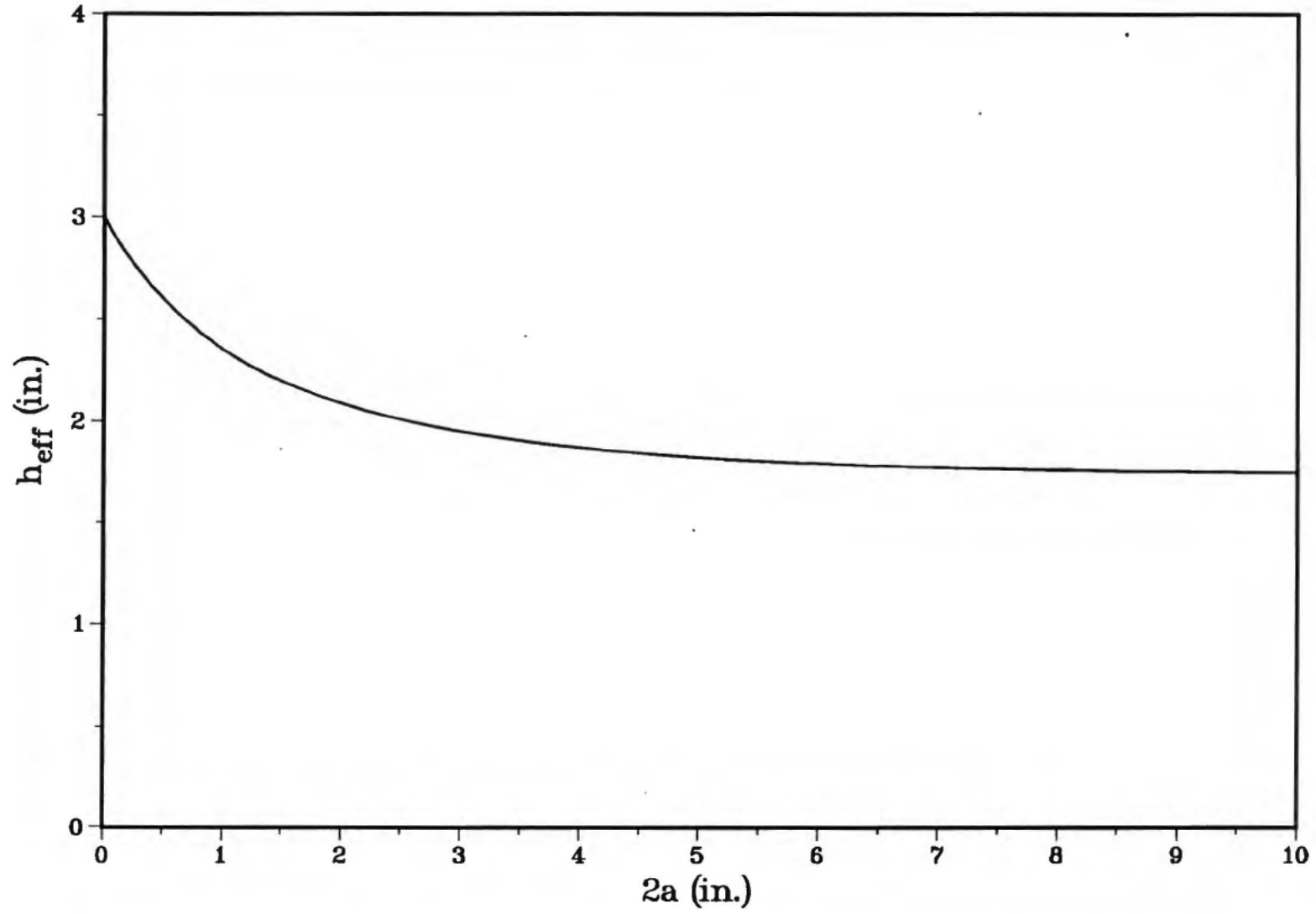
Figure 16.   Effective height of a conducting tube (h = 6 in.) above a ground plane (s = 0.1 in.) as a function of diameter.
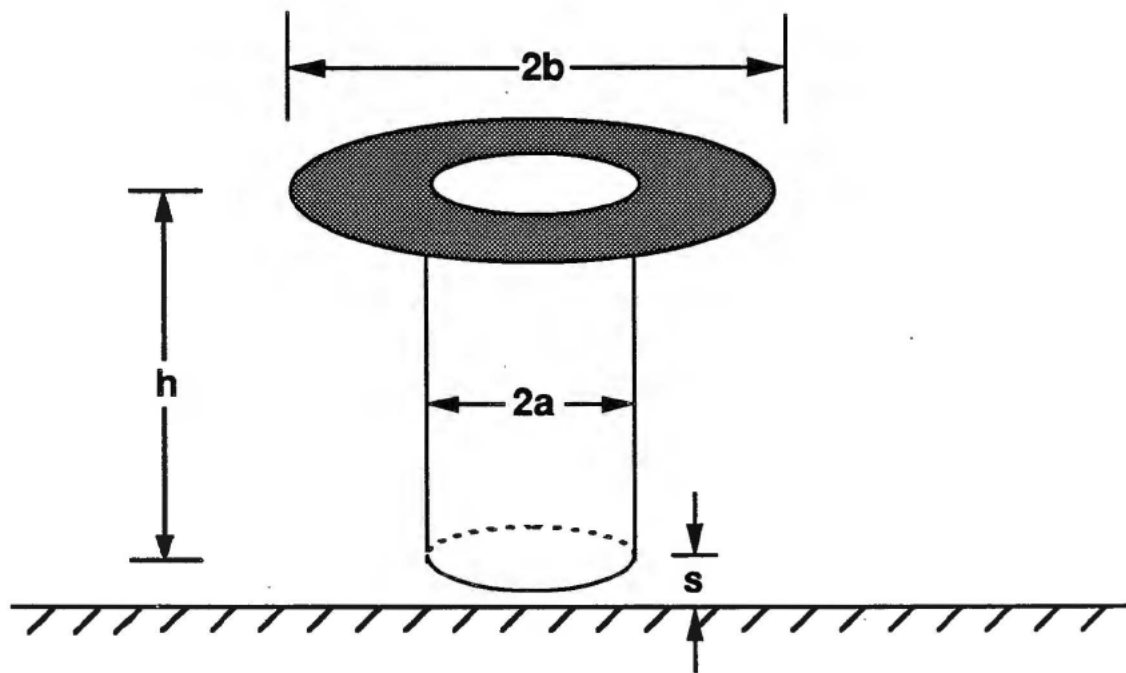
Figure 17.   Top-loaded conducting tube above a ground plane.
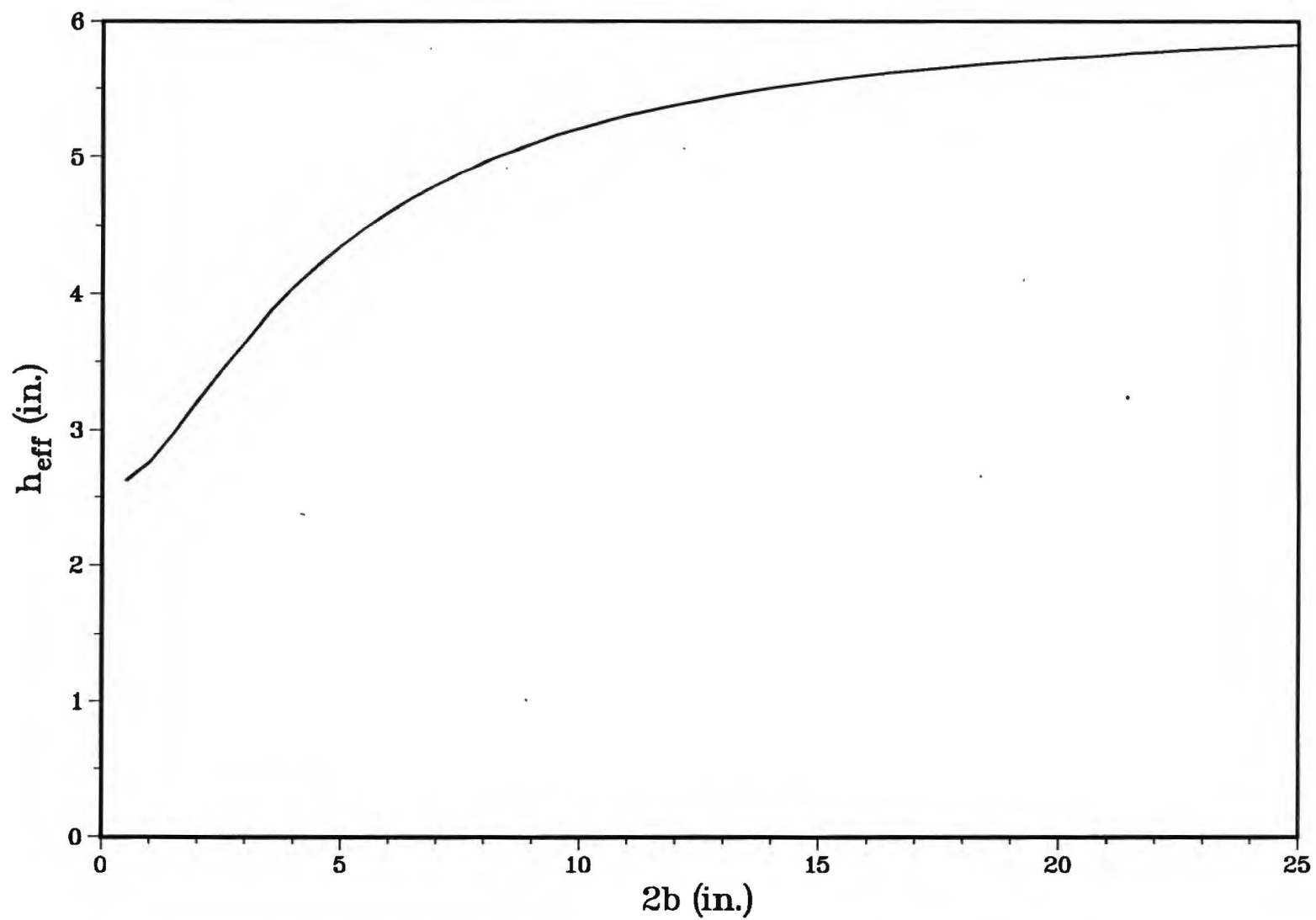
Figure 18.   Effective height of a top-loaded conducting tube (h = 6 in., 2a = 0.5 in.) above a ground plane (s = 0.1 in.) as a function of the top-load outer diameter.
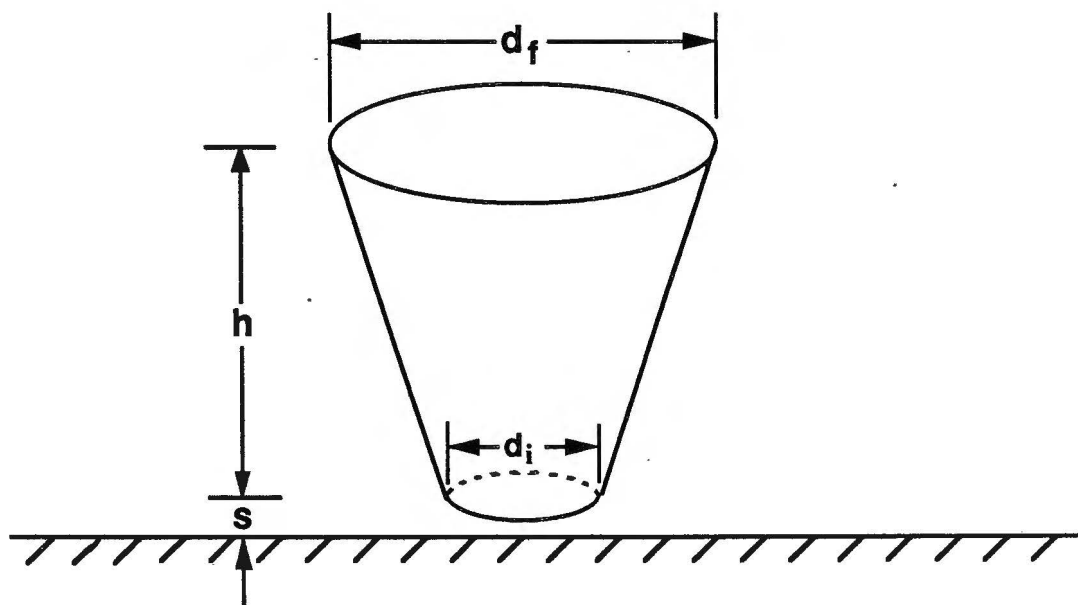
Figure 19.   Truncated cone above a ground plane.
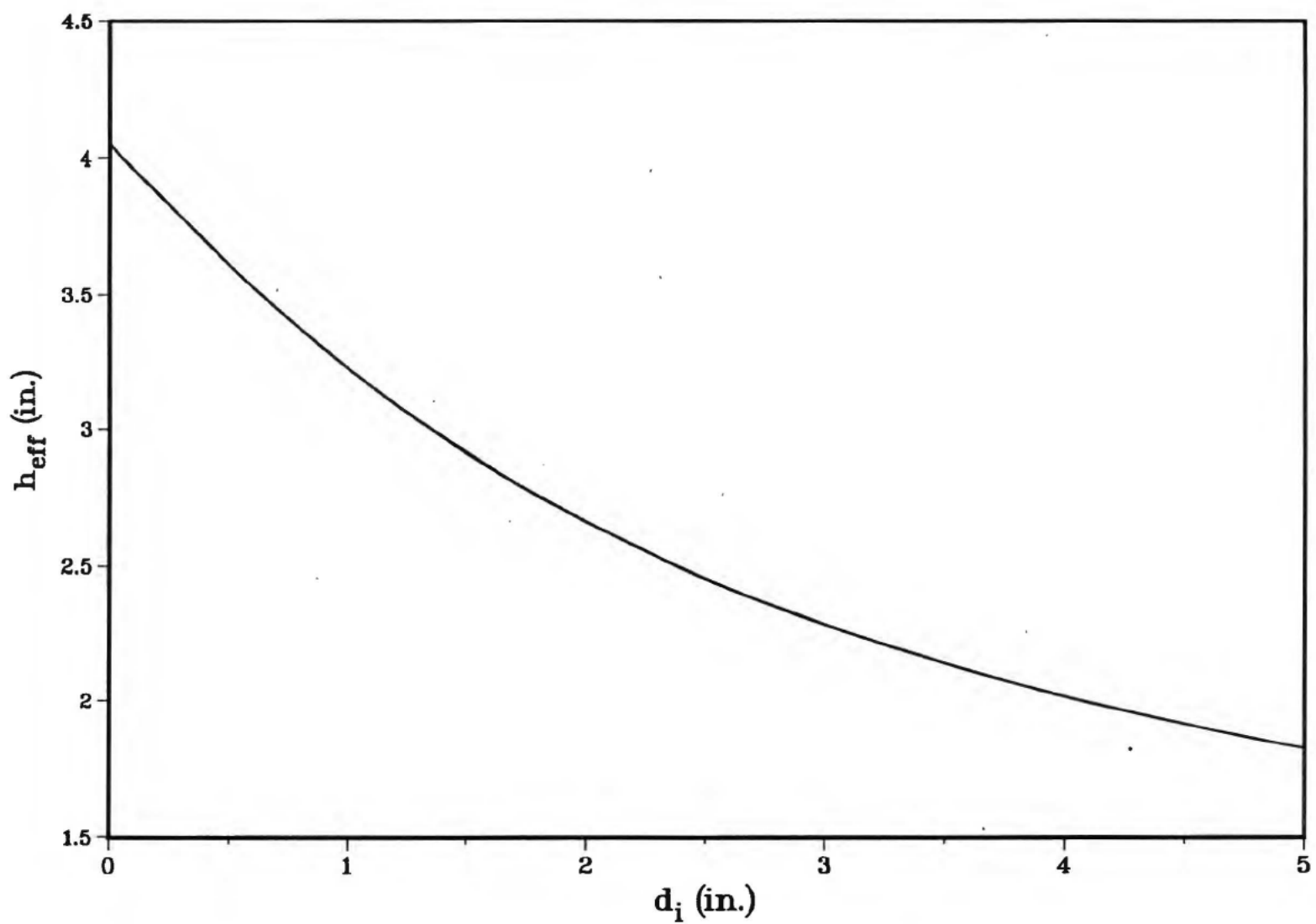
Figure 20.   Effective height of a truncated cone (h = 6 in., d_f = 5 in.) above a ground plane (s = 0.1 in.) as a function of the lower diameter.
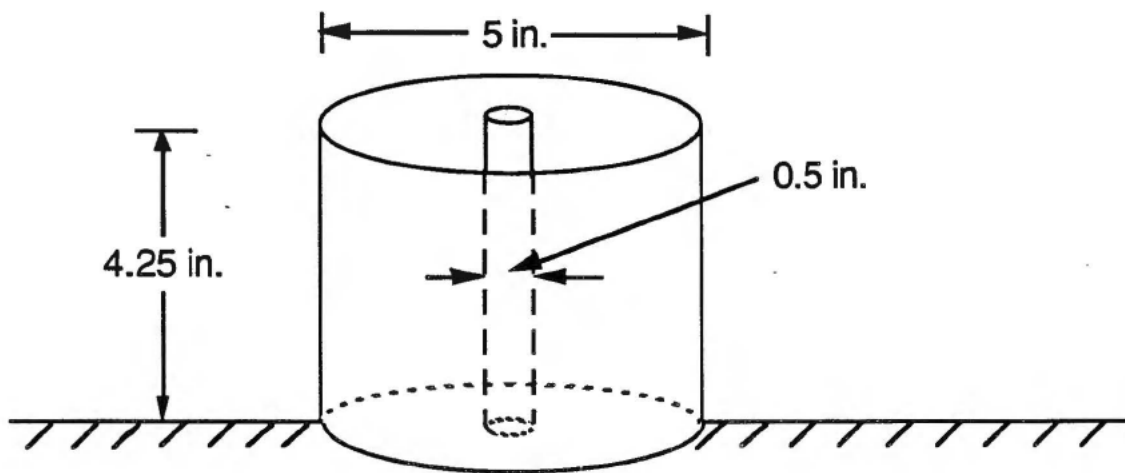
Figure 21   Space restrictions for the Loran-C antenna.
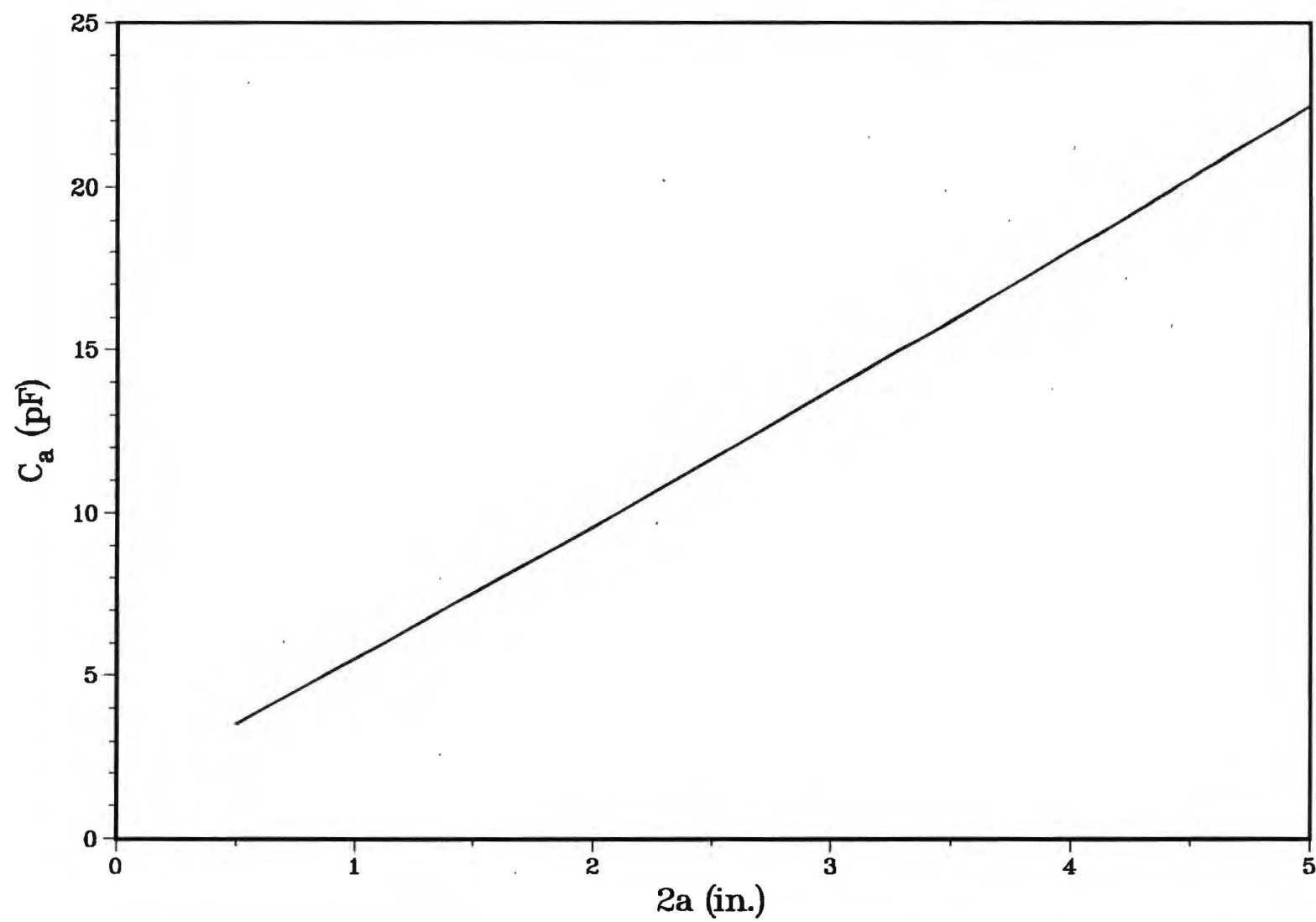
Figure 22a.   Capacitance of a conducting tube (h = 4.15 in.) above a ground plane (s = 0:1 in.) as a function of diameter.
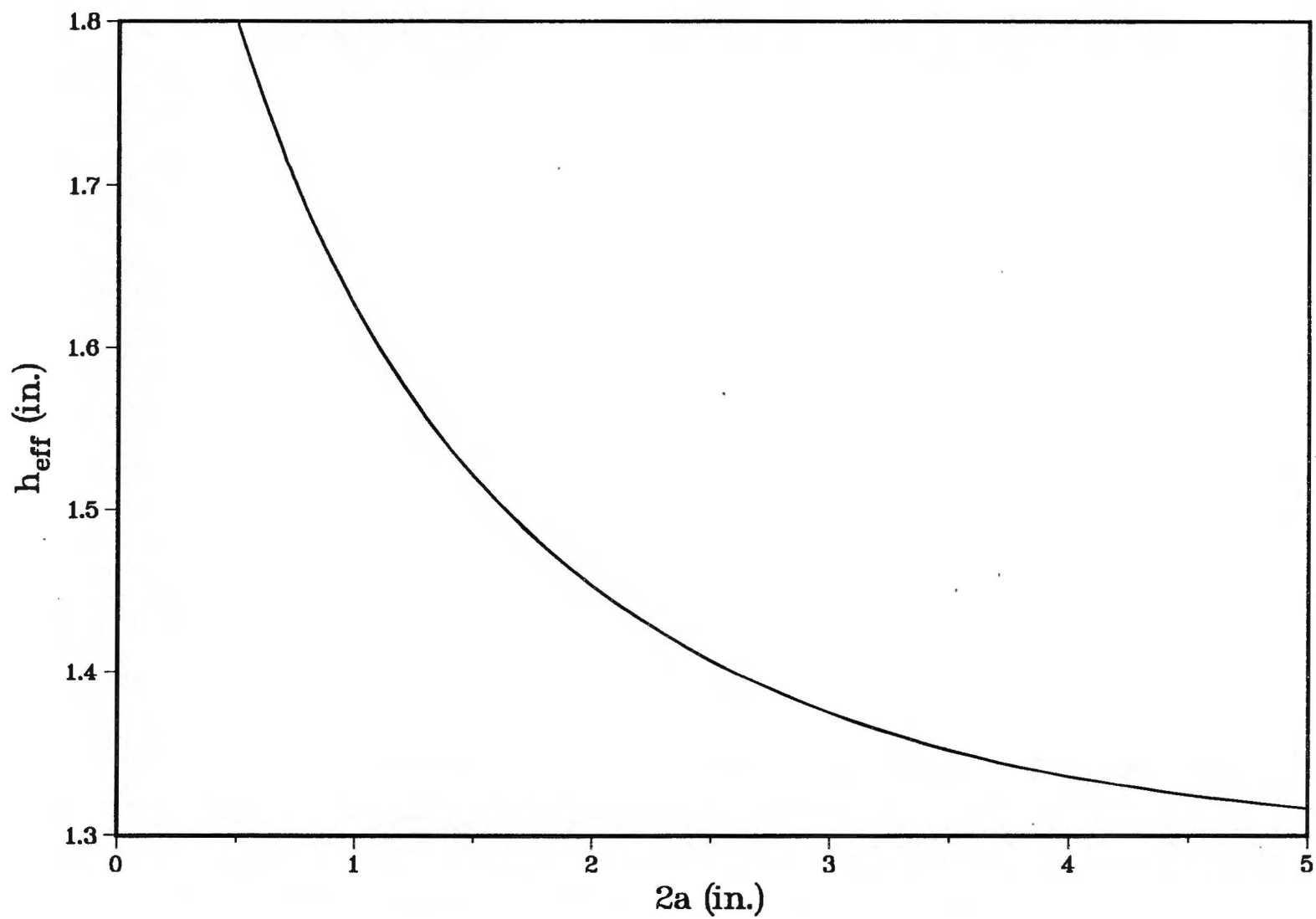
Figure 22b.   Effective height of a conducting tube (h = 4.15 in.) above a ground plane (s = 0.1 in.) as a function of diameter.
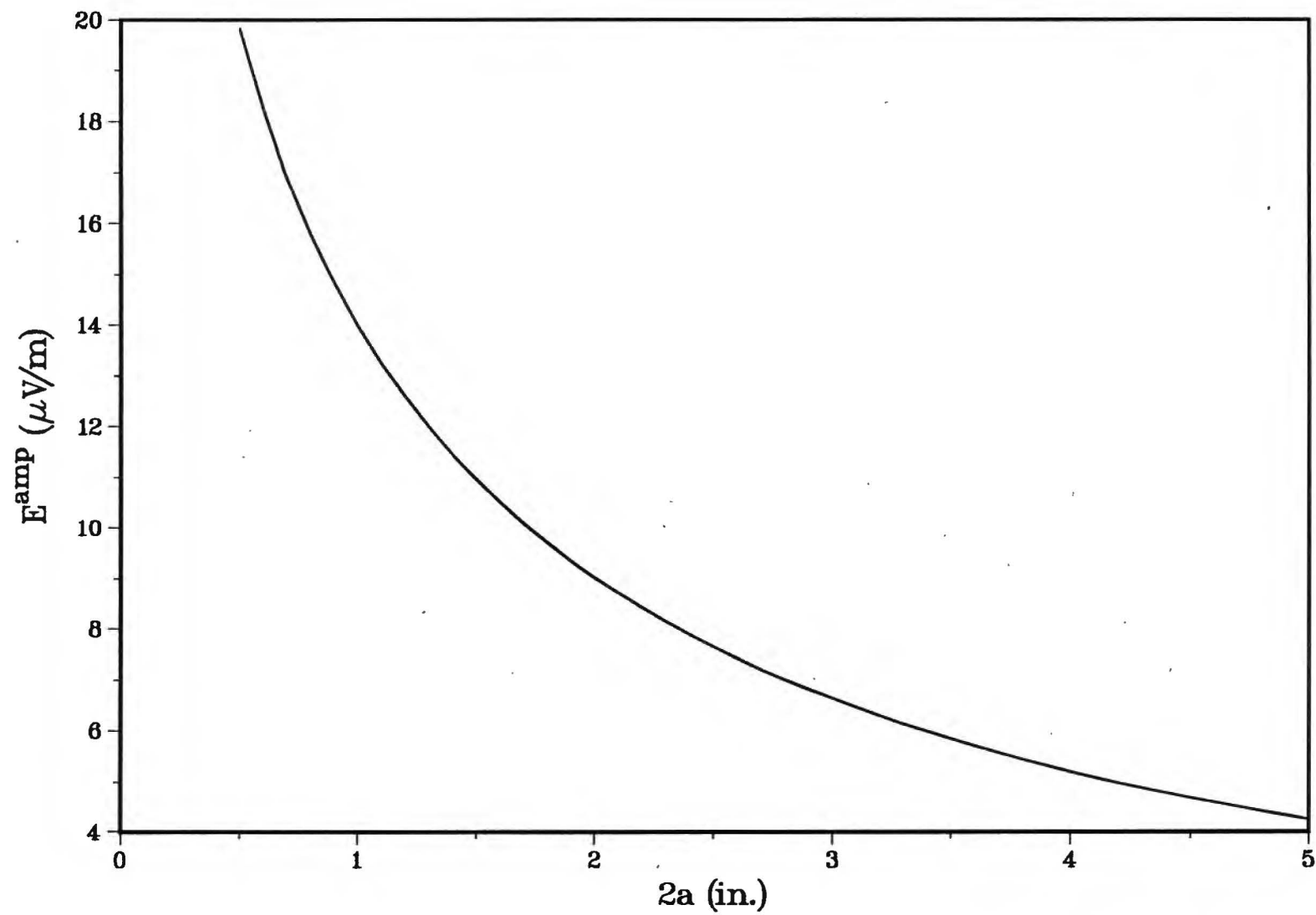
Figure 22c. Amplifier noise field due to a current noise limited FET (I_n = 2 pA, f = 100 kHz) for the conducting tube described in Fig. 22a and plotted as a function of the tube diameter.
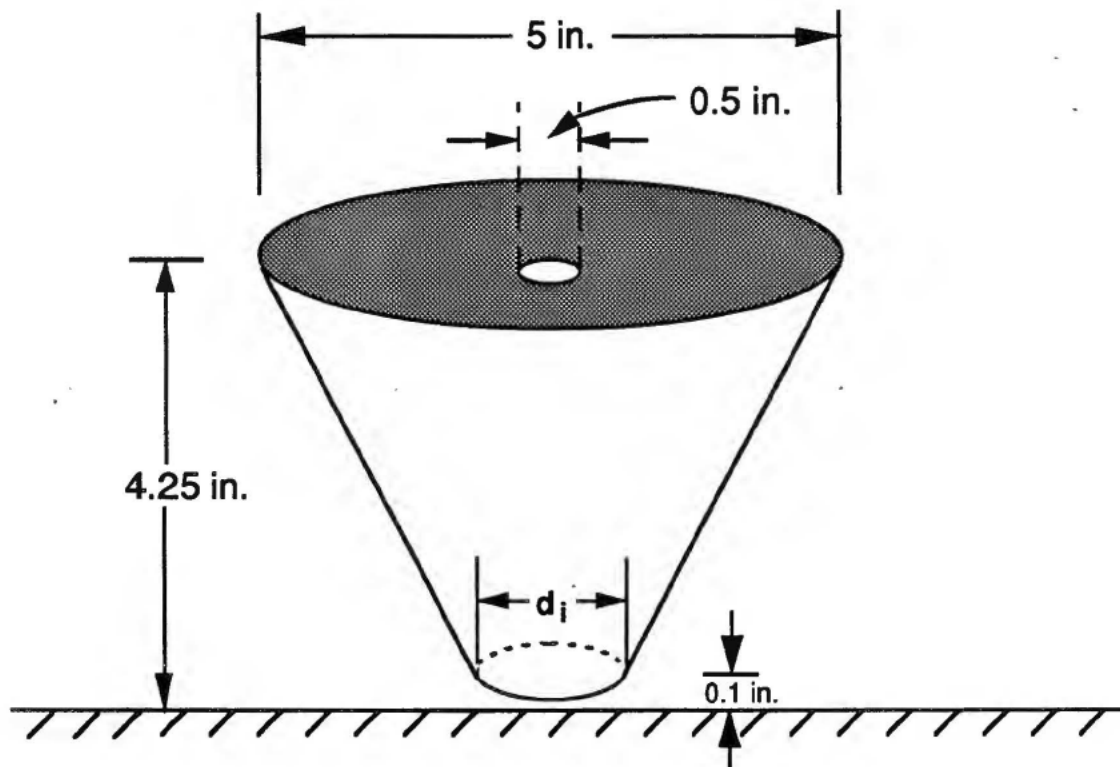
Figure 23.   Top-loaded truncated cone above a ground plane.
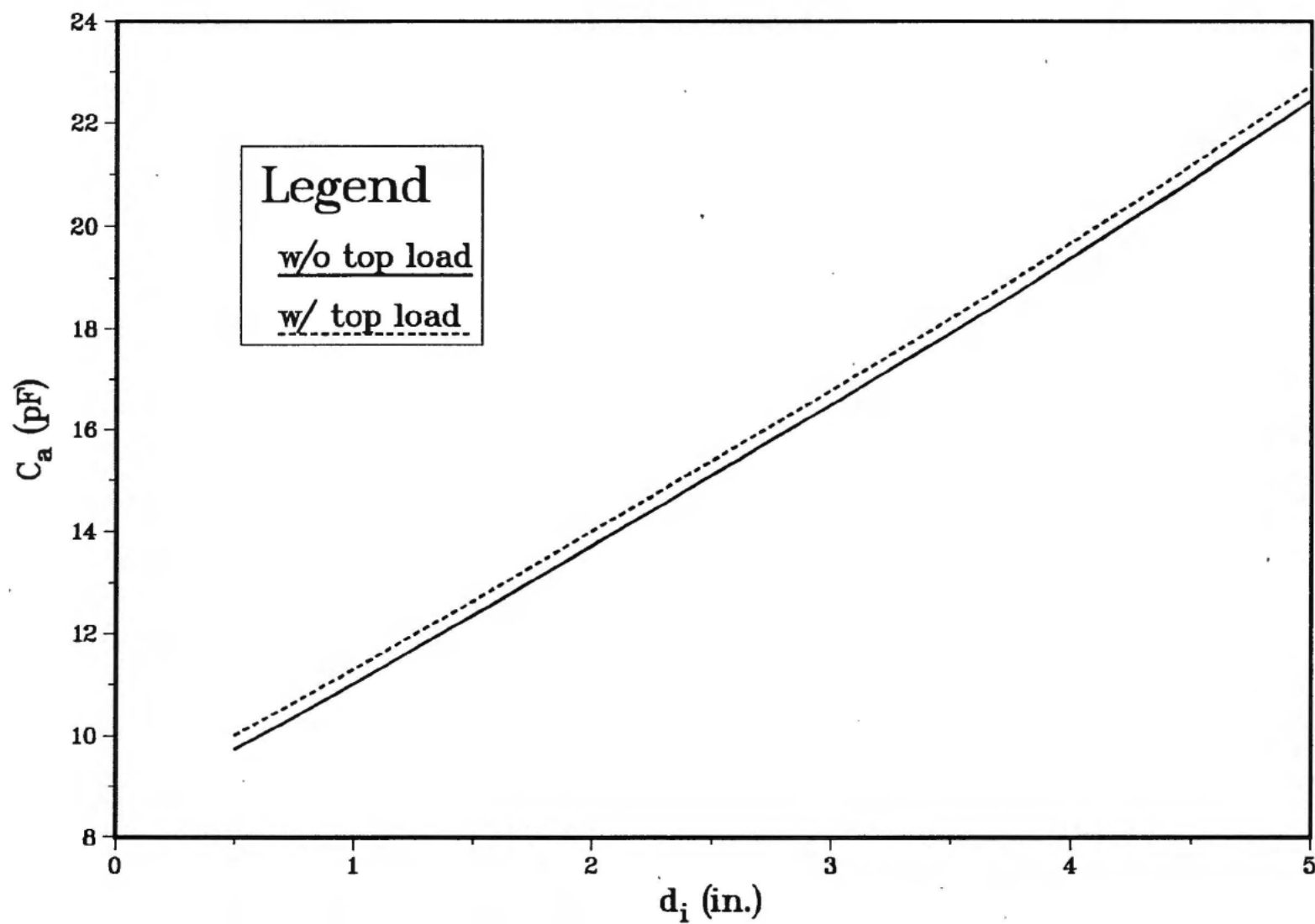
Figure 24a.   Capacitance of the truncated cone described in Fig. 23 as a function of the lower diameter.
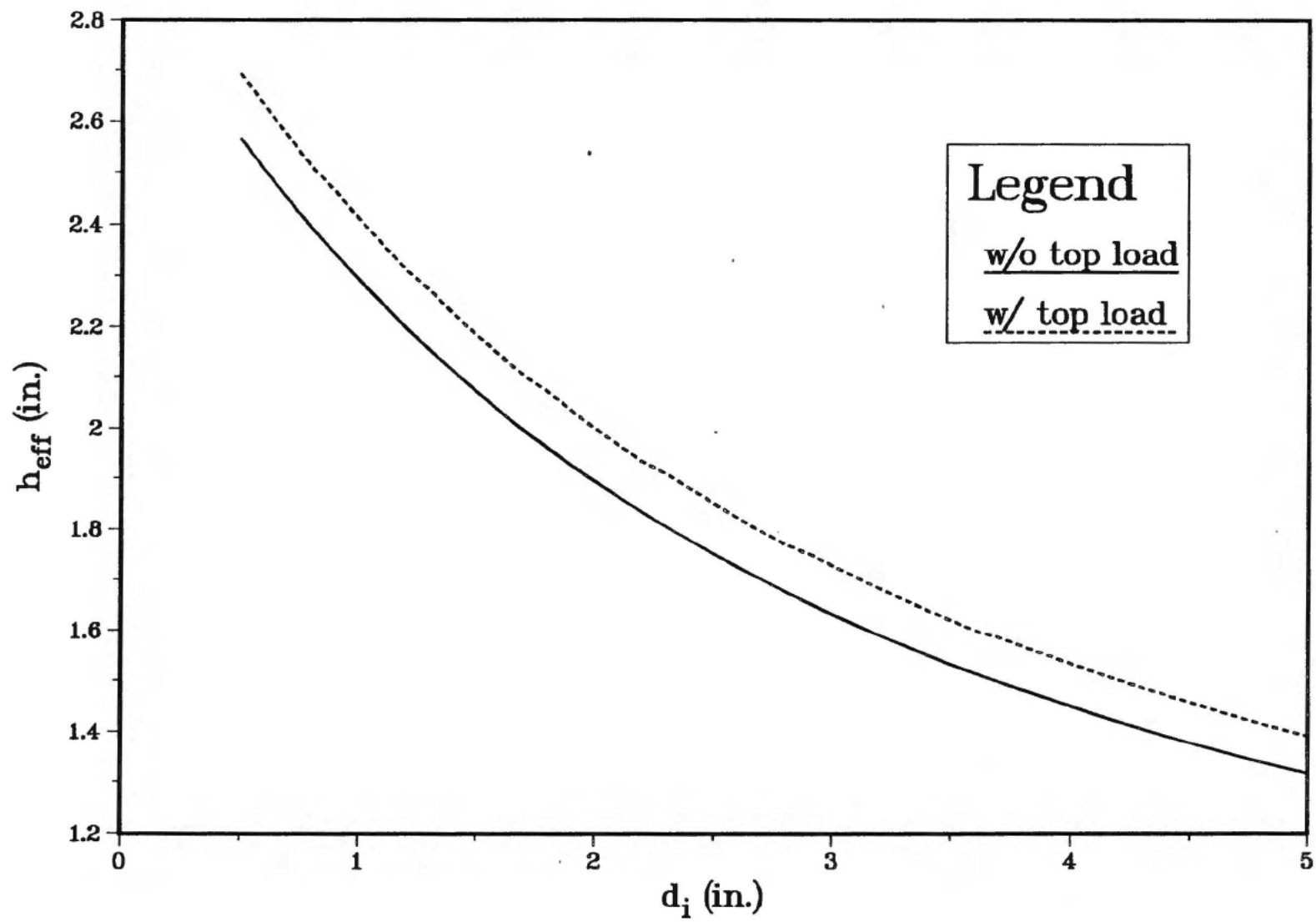
Figure 24b. Effective height of the truncated cone described in Fig. 23 as a function of the lower diameter.
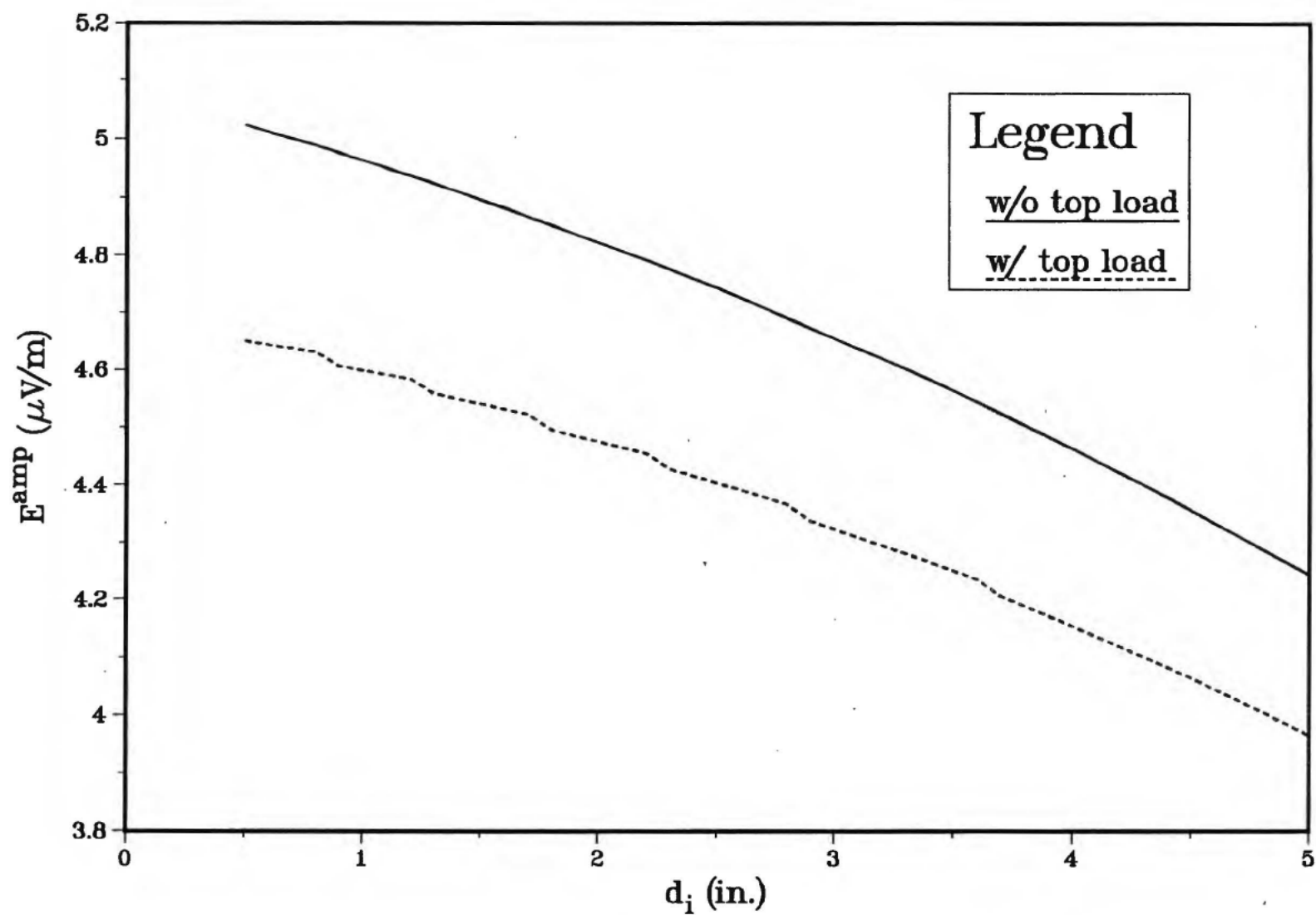
Figure 24c. Amplifier noise field due to a current noise limited FET (I_n = 2 pA, f = 100 kHz) for the truncated cone described in Fig. 23 and plotted as a function of the lower diameter.
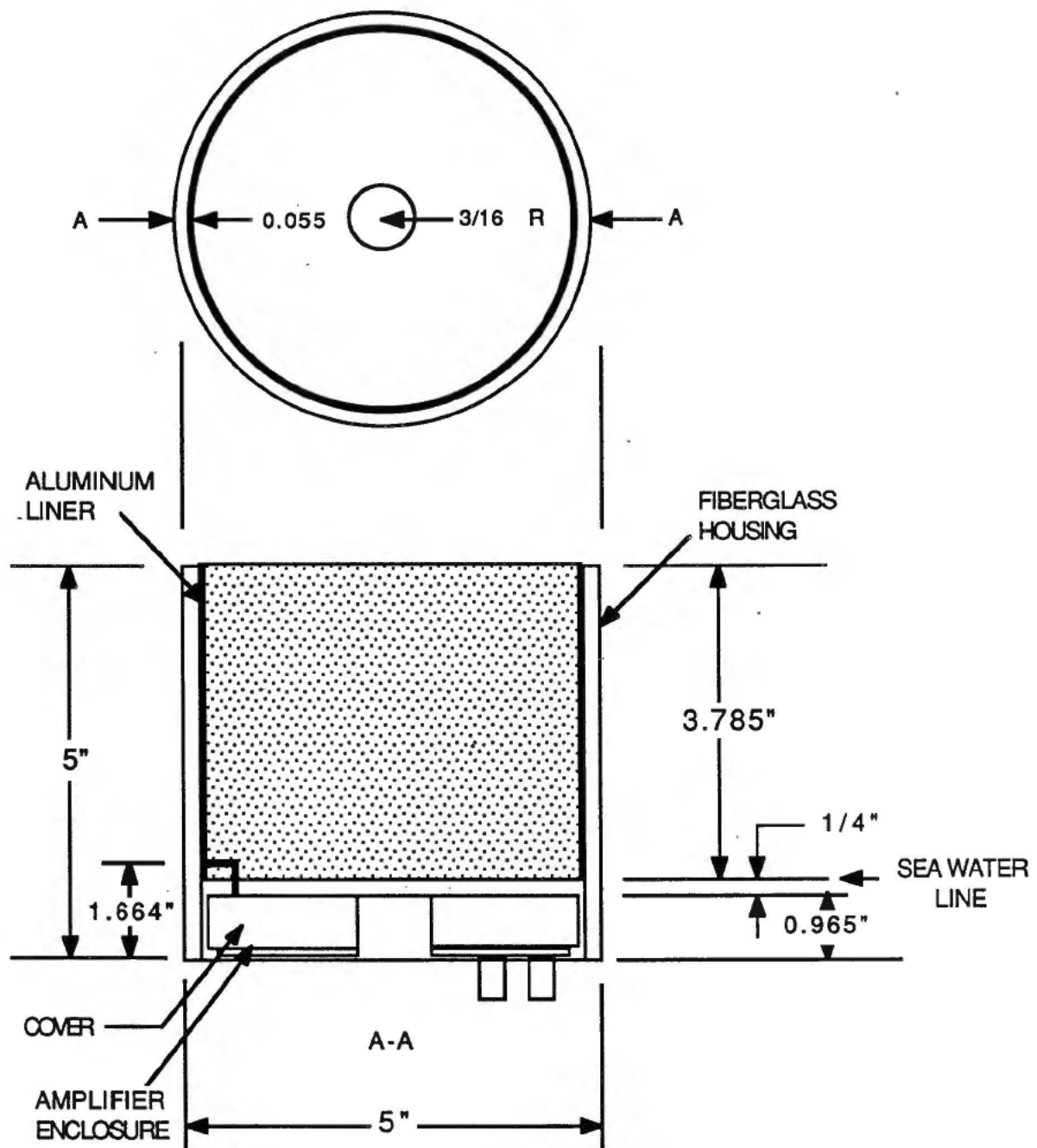
Figure 25. Schematic view of the Loran-C antenna.

APPENDIX A

ANALYSIS OF THE SINGULARITY IN THE INTEGRAND OF EQN. (18)

In this analysis, the following parametrization is valid:

$$z - z' = (t - t') \cos v_j \qquad (A-1a)$$

$$\rho - \rho' = (t - t') \sin v_j \qquad (A-1b)$$

where v_j is defined by (23). From (14),

$$\frac{K(u^2)}{R_1^+} = \frac{1}{2} \int_0^\pi \frac{1}{R^+} d\phi'$$

$$= \frac{1}{2\sqrt{\rho\rho'}} \int_0^{\pi/2} \frac{d\alpha}{\sqrt{\gamma^2 + \sin^2\alpha}} \qquad (A-2)$$

where

$$\gamma = \frac{\left[(\rho-\rho')^2 + (z-z')^2\right]^{1/2}}{2\sqrt{\rho\rho'}} = \frac{|t-t'|}{2\sqrt{\rho\rho'}} \qquad (A-3)$$

It is desired to determine the above integral when $t' \to t$ ($\gamma \to 0$). As $t' \to t$, the latter integrand in

(A–2) is singular when $\alpha = 0$. Equation (A–2) may be expressed as

$$\frac{K(u^2)}{R_1^+} = \frac{1}{2\sqrt{\rho\rho'}} \left(I_b(\gamma) + I_s(\gamma)\right) \qquad (A-4)$$

where

$$I_b(\gamma) = \int_0^{\pi/2} \frac{1 - \cos\alpha}{\sqrt{\gamma^2 + \sin^2\alpha}} d\alpha \qquad (A-5a)$$

$$I_s(\gamma) = \int_0^{\pi/2} \frac{\cos\alpha}{\sqrt{\gamma^2 + \sin^2\alpha}} d\alpha \qquad (A-5b)$$

The integrand of $I_b(\gamma)$ is bounded for $\gamma = 0$ and $\alpha = 0$ while the integrand of $I_s(\gamma)$ is singular.

An evaluation of I_b at $\gamma = 0$ is given as follows:

$$\lim_{\gamma \to 0} I_b(\gamma) = \int_0^{\pi/2} \frac{1 - \cos \alpha}{\sin \alpha} \, d\alpha = \ln\left(\frac{1 - \cos \alpha}{\sin^2 \alpha}\right)\Bigg|_{\alpha = 0}^{\alpha = \pi/2}$$

$$= \lim_{\alpha \to 0} \ln\left(\frac{\sin^2 \alpha}{1 - \cos \alpha}\right) = \ln(2) \tag{A-6}$$

The substitution of $x = \sin \alpha$ in (A–5b) gives

$$I_s(\gamma) = \int_0^1 \frac{1}{\sqrt{\gamma^2 + x^2}} \, dx = \ln\left(x + \sqrt{x^2 + \gamma^2}\right)\Bigg|_{x=0}^{x=1} = -\ln\left(\frac{\gamma}{1 + \sqrt{1 + \gamma^2}}\right)$$

Therefore,

$$\lim_{\gamma \to 0} I_s(\gamma) = -\ln\left(\frac{|\gamma|}{2}\right) \tag{A-7}$$

Thus I_s has a logarithmic singularity at $\gamma = 0$. From (A–6) and (A–7),

$$\lim_{\gamma \to 0} \left(I_b(\gamma) + I_s(\gamma)\right) = -\ln\left(\frac{|\gamma|}{4}\right) = -\ln\left(\frac{|t - t'|}{8\rho}\right) \tag{A-8}$$

The use of (A–8) in (A–4) yields

$$\lim_{t' \to t} \frac{K(u^2)}{R_1^+} = \frac{1}{2\rho} \lim_{\gamma \to 0} \left(I_b(\gamma) + I_s(\gamma)\right)$$

$$= -\frac{1}{2\rho} \ln\left(\frac{|t - t'|}{8\rho}\right)$$

$$= \frac{1}{2\rho}\left[\ln(4) + \ln(2\rho) - \ln|t - t'|\right] \tag{A-9}$$

A similar result was obtained by Glisson and Wilton [11] in their study of electromagnetic scattering from bodies of revolution.

APPENDIX B

COMPUTER PROGRAM

The double precision FORTRAN computer program listed in this appendix computes the charge distribution, input capacitance, and effective height of a conducting body of revolution above a conducting ground plane. The charge distribution along the body is obtained from the solution of (18) by the method of moments as described in this report. The capacitance is given by (19) while the effective height is obtained from (46). In addition, the amplifier noise field is determined from (7).

The endpoints of the segments approximating the generating curve ($(\bar{\rho}_i, \bar{z}_i)$, i = 0, 1, 2, ..., N) of the body of revolution are read from a data file. The coefficient matrix S has elements given by (28) for i ≠ j and (34) for i = j that involve integrals with the following integrands:

$$\text{FINT} = \frac{K(u_{ij}^2)}{R_{ij}^+}, \quad i \neq j \tag{B-1}$$

$$\text{FINTD} = \frac{K(u_{ii}^2)}{R_{ii}^+} + \frac{1}{2\rho_i} \ln \left| \frac{\Delta_i}{2} - \tau' \right| \tag{B-2}$$

$$\text{FINTI} = \frac{K(w_{ij}^2)}{R_{ij}^-} \tag{B-3}$$

where all variables were previously defined while K is the complete elliptic integral of the first kind. The function ELIPT computes K by a polynomial approximation given in [5]. The above integrands are functions of τ'. Special care is taken so that FINTD is not evaluated at $\tau' = \Delta_i/2$. The integrals are computed by calling the function SIMP. SIMP computes the integral of a real function with finite limits by Simpson's rule with automatic halving. The relative error for the integrations is given by REL. In this study, REL was set at 10^{-4} for 4-place accuracy.

The linear system of equations, given in matrix form by (35), is solved for the unknown

charge density vector Q by calling the subroutines FACTR and SOLVE. FACTR factors the coefficient matrix S into the product of a lower triangular matrix and an upper triangular matrix using the Gauss-Doolittle algorithm [12]. The factored matrix is used by SOLVE to determine the solution of the matrix equation. The excitation vector is read into Q and is overwritten with the charge density vector after calling SOLVE. FACTR and SOLVE are part of the Numerical Electromagnetics Code [13].

```
C  ********************************************************************
C     THIS PROGRAM COMPUTES THE ELECTROSTATIC CHARGE PER UNIT LENGTH OF A
C     CONDUCTING BODY OF REVOLUTION CHARGED TO A CONSTANT POTENTIAL AND LYING
C     ABOVE A CONDUCTING GROUND PLANE. AN INTEGRAL EQUATION IS SOLVED FOR THE
C     CHARGE DENSITY BY THE METHOD OF MOMENTS USING PULSE EXPANSION FUNCTIONS
C     AND POINT MATCHING. THE RESULT IS APPLIED TO EVALUATE THE CAPACITANCE,
C     EFFECTIVE HEIGHT, AND AMPLIFIER NOISE FIELD OF AN ELECTRICALLY SMALL
C     ANTENNA CONSISTING OF THE BODY OF REVOLUTION AND AN INFINITESIMALLY THIN
C     WIRE CONNECTING THE BODY TO A RECEIVER LOCATED BELOW THE GROUND PLANE.
C
C     THE INPUT VARIABLES ARE GIVEN AS FOLLOWS:
C         REL = RELATIVE ERROR FOR INTEGRATIONS
C        VOLT = POTENTIAL OF BODY IN VOLTS
C          CW = INTERCONNECTION CAPACITANCE IN PICOFARADS
C       NVOLT = AMPLIFIER NOISE VOLTAGE IN NANOVOLTS
C        NCUR = AMPLIFIER NOISE CURRENT IN PICOAMPS
C           N = NO. OF BASIS FUNCTIONS
C     RHOB(I) = RADIAL COORDINATE OF ENDPOINT I IN INCHES
C       ZB(I) = AXIAL COORDINATE OF ENDPOINT I IN INCHES
C
C     INTERMEDIATE VARIABLES ARE GIVEN AS FOLLOWS:
C      RHO(I) = RADIAL COORDINATE OF MIDPOINT OF SEGMENT I IN METERS
C        Z(I) = AXIAL COORDINATE OF MIDPOINT OF SEGMENT I IN METERS
C        T(I) = T COORDINATE OF MIDPOINT OF SEGMENT I IN METERS
C        D(I) = LENGTH OF SEGMENT I IN METERS
C        V(I) = ANGLE BETWEEN SEGMENT I AND THE Z-AXIS
C      S(I,J) = (I,J) ELEMENT OF COEFFICIENT MATRIX
C
C     THE OUTPUT VARIABLES ARE GIVEN AS FOLLOWS:
C        Q(I) = CHARGE DENSITY ALONG MIDPOINT OF SEGMENT I IN COUL/M
C         CAP = ANTENNA CAPACITANCE IN FARADS
C          EH = ANTENNA EFFECTIVE HEIGHT IN METERS
C        EAMP = AMPLIFIER NOISE FIELD IN VOLTS/M
C  ********************************************************************
C
      IMPLICIT REAL*8 (A-H,O-Z)
      REAL*8 NCUR,NVOLT
      DIMENSION RHO(200),RHOB(0:200),Z(200),ZB(0:200),T(200),V(200),D(200)
      DIMENSION Q(200),S(200,200),IP(200)
      EXTERNAL FINT,FINTD,FINTI,ELIPT
      COMMON /C1/ RI,RJ1,ZI,ZJ1,CVJ,SVJ,DI2
C
C     **** CONSTANTS ****
C
      PI=3.14159265358979D0
      E0=8.854D-12    ! PERMITTIVITY OF FREE SPACE
      VOLT=1.D0    ! POTENTIAL IN VOLTS
      FR=1.D+5     ! FREQUENCY
C
C     **** READ INPUT DATA ****
C
      WRITE(6,1)
      WRITE(7,1)
    1 FORMAT(10X,'BODY OF REVOLUTION ABOVE A CONDUCTING GROUND PLANE')
      WRITE(6,10)
   10 FORMAT(/,5X,'ENTER RELATIVE ERROR FOR INTEGRATIONS : ',$)
      READ(6,*) REL
      WRITE(7,15) REL
```

```
 15   FORMAT(10X,'RELATIVE ERROR FOR INTEGRATIONS = ',E12.5)
      WRITE(6,20)
 20   FORMAT(/,5X,'ENTER POTENTIAL OF BODY IN VOLTS : ',$)
      READ(6,*) VOLT
      WRITE(7,25) VOLT
 25   FORMAT(/,5X,'POTENTIAL OF BODY = ',E12.5,' VOLTS')
      WRITE(6,30)
 30   FORMAT(/,5X,'ENTER INTERCONNECTION CAPACITANCE IN PICOFARADS',
     *       ' : ',$)
      READ(6,*) CW
      WRITE(7,35) CW
 35   FORMAT(/,5X,'INTERCONNECTION CAPACITANCE = ',E12.5,' PICOFARADS')
      CW=CW*1.D-12
      WRITE(6,40)
 40   FORMAT(/,5X,'ENTER AMPLIFIER NOISE VOLTAGE IN NANOVOLTS : ',$)
      READ(6,*) NVOLT
      WRITE(7,45) NVOLT
 45   FORMAT(/,5X,'AMPLIFIER NOISE VOLTAGE = ',E12.5,' NANOVOLTS')
      NVOLT=NVOLT*1.D-9
      WRITE(6,50)
 50   FORMAT(/,5X,'ENTER AMPLIFIER NOISE CURRENT IN PICOAMPS : ',$)
      READ(6,*) NCUR
      WRITE(7,55) NCUR
 55   FORMAT(/,5X,'AMPLIFIER NOISE CURRENT = ',E12.5,' PICOAMPS')
      NCUR=NCUR*1.D-12
      READ(8,60) N    ! READ NO. OF SEGMENTS
 60   FORMAT(1X,I3)
      WRITE(7,65)
 65   FORMAT(/,5X,'NO. OF SEGMENTS = ',I3)
      DO 70 I=0,N    ! READ SEGMENT ENDPOINTS
      READ(8,80) RHOB(I),ZB(I)
 80   FORMAT(1X,E22.15,5X,E22.15)
 70   CONTINUE
C
      DO 100 I=0,N    ! CONVERT SEGMENT ENDPOINTS TO METERS
      RHOB(I)=RHOB(I)*2.54D-2
 100  ZB(I)=ZB(I)*2.54D-2
      DO 110 I=1,N
      RHO(I)=(RHOB(I-1)+RHOB(I))*.5D0
      Z(I)=(ZB(I-1)+ZB(I))*.5D0
      V(I)=ATAN2(RHOB(I)-RHOB(I-1),ZB(I)-ZB(I-1))
      D(I)=SQRT((RHOB(I)-RHOB(I-1))**2+(ZB(I)-ZB(I-1))**2)
      IF (I.EQ.1) THEN
         T(I)=.5D0*D(I)
      ELSE
         T(I)=T(I-1)+.5D0*(D(I-1)+D(I))
      END IF
 110  CONTINUE
C
C     **** EVALUATE COEFFICIENT MATRIX ****
C
      DO 200 I=1,N
      RI=RHO(I)
      ZI=Z(I)
      DI2=.5D0*D(I)
      DO 210 J=1,N
      RJ1=RHOB(J-1)
      ZJ1=ZB(J-1)
```

```
        CVJ=COS(V(J))
        SVJ=SIN(V(J))
        SIMAGE=SIMP(FINTI,0.D0,D(J),REL)
        IF (I.EQ.J) GO TO 220
        S(I,J)=SIMP(FINT,0.D0,D(J),REL)-SIMAGE
        GO TO 210
220     EP=DI2*1.D-2
        EPL=DI2-EP
        EPU=DI2+EP
        ST=SIMP(FINTD,0.D0,EPL,REL)+SIMP(FINTD,EPU,D(I),REL)
        DO 230 L=1,5
        EP=EP*.1D0
        EPL1=DI2-EP
        EPU1=DI2+EP
        ST1=SIMP(FINTD,EPL,EPL1,REL)+SIMP(FINTD,EPU1,EPU,REL)+ST
        IF (ABS(ST1-ST).LT.REL*ABS(ST)) THEN
            S(I,I)=ST1+DI2*(1.D0-LOG(DI2))/RHO(I)-SIMAGE
            GO TO 210
        ELSE
            ST=ST1
            EPL=EPL1
            EPU=EPU1
        END IF
230     CONTINUE
        S(I,I)=ST1+DI2*(1.D0-LOG(DI2))/RHO(I)-SIMAGE
        WRITE(6,240) I,I
240     FORMAT(//,10X,'S(',I3,',',I3,') IS NOT ACCURATE!')
210     CONTINUE
200     CONTINUE
C
C       **** COMPUTE INPUT EXCITATION VECTOR ****
C
        TEMP=2.D0*PI*PI*E0*VOLT
        DO 250 I=1,N
250     Q(I)=TEMP
C
C       **** COMPUTE CHARGE DISTRIBUTION ****
C
        CALL FACTR(N,S,IP,200)
        CALL SOLVE(N,S,IP,Q,200)
C
C       **** COMPUTE CAPACITANCE ****
C
        QT=0.D0
        DO 260 I=1,N
260     QT=QT+Q(I)*D(I)     ! TOTAL CHARGE ALONG BODY
        CAP=QT/VOLT
C
C       **** COMPUTE EFFECTIVE HEIGHT ****
C
        EH=0.D0
        DO 270 I=1,N
270     EH=EH+Q(I)*D(I)*(Z(I)-ZB(0))
        EH=EH/QT
        EH=EH+ZB(0)     ! ACCOUNT FOR HEIGHT OF CONNECTING WIRE
C
        EAMP=(NVOLT*(1.D0+CW/CAP))**2+(NCUR/(2.D0*PI*FR*CAP))**2
        EAMP=SQRT(EAMP)/EH  ! AMPLIFIER NOISE FIELD IN VOLTS/METER
```

```
C
C     **** PRINT OUTPUT ****
C
      WRITE(7,300) (I,T(I)/2.54D-2,I,Q(I),I=1,N)
 300  FORMAT(1X,'T(',I3,') = ',E14.7,' in.',5X,'Q(',I3,') = ',E14.7,
     *   'COUL/M')
      WRITE(7,310) CAP*1.D+12
 310  FORMAT(10X,'CAPACITANCE = ',E14.7,' pF')
      WRITE(7,320) EH/2.54D-2
 320  FORMAT(10X,'EFFECTIVE HEIGHT = ',E14.7,' in.')
      WRITE(7,330) EAMP*1.D+6
 330  FORMAT(10X,'AMPLIFIER NOISE FIELD = ',E14.7,' microvolts/m')
      STOP
      END
C
C
      FUNCTION FINT(T)
      IMPLICIT REAL*8 (A-H,M-Z)
      COMMON /C1/ RI,RJ1,ZI,ZJ1,CVJ,SVJ,DI2
      R2=SQRT((RI+RJ1+T*SVJ)**2+(ZI-ZJ1-T*CVJ)**2)
      U2=4.D0*RI*(RJ1+T*SVJ)/(R2**2)
      M1=1.D0-U2
      FINT=ELIPT(M1)/R2
      RETURN
      END
C
C
      FUNCTION FINTD(T)
      IMPLICIT REAL*8 (A-H,M-Z)
      COMMON /C1/ RI,RJ1,ZI,ZJ1,CVJ,SVJ,DI2
      R2=SQRT((RI+RJ1+T*SVJ)**2+(ZI-ZJ1-T*CVJ)**2)
      U2=4.D0*RI*(RJ1+T*SVJ)/(R2**2)
      M1=1.D0-U2
      FINTD=ELIPT(M1)/R2+.5D0*LOG(ABS(DI2-T))/RI
      RETURN
      END
C
C
      FUNCTION FINTI(T)
      IMPLICIT REAL*8 (A-H,M-Z)
      COMMON /C1/ RI,RJ1,ZI,ZJ1,CVJ,SVJ,DI2
      R3=SQRT((RI+RJ1+T*SVJ)**2+(ZI+ZJ1+T*CVJ)**2)
      G2=4.D0*RI*(RJ1+T*SVJ)/(R3**2)
      M1=1.D0-G2
      FINTI=ELIPT(M1)/R3
      RETURN
      END
C
C
      FUNCTION ELIPT(AM1)
C     ************************************************************
C     COMPLETE ELLIPTIC INTEGRAL OF THE FIRST KIND,K(M),AS DEFINED
C          IN THE REFERENCE BELOW,WHERE AM1=1-M .
C
C     REFERENCE: HANDBOOK OF MATHEMATICAL FUNCTIONS (AMS-55)
C     AUTHORS: ABRAMOWITZ AND STEGUN
C     EQ. 17.3.34
C     ************************************************************
```

```
      IMPLICIT REAL*8 (A-H,O-Z)
      DATA A0,A1,A2,A3,A4,B0,B1,B2,B3,B4/1.38629436112D0,
     *      .9666344259D-1,.3590092383D-1,.3742563713D-1,
     *       .1451196212D-1,.5D0,.12498593597D0,.6880248576D-1,
     *       .3328355346D-1,.441787012D-2/
      A=A0+A1*AM1
      B=B0+B1*AM1
      IF (AM1.LT.1.D-18) GO TO 10
      AM12=AM1*AM1
      A=A+A2*AM12
      B=B+B2*AM12
      IF (AM1.LT.1.D-12) GO TO 10
      AM13=AM12*AM1
      A=A+A3*AM13
      B=B+B3*AM13
      IF (AM1.LT.1.D-9) GO TO 10
      AM14=AM13*AM1
      A=A+A4*AM14
      B=B+B4*AM14
   10 CONTINUE
      ELIPT=A-B*LOG(AM1)
      RETURN
      END
C
C

      FUNCTION SIMP(F,A,B,REL)
C     **********************************************************
C     INTEGRATION BY SIMPSON'S RULE WITH AUTOMATIC HALVING
C     **********************************************************
C       F = REAL FUNCTION TO BE INTEGRATED
C       A = LOWER LIMIT OF INTEGRATION
C       B = UPPER LIMIT OF INTEGRATION
C     REL = RELATIVE ERROR INDICATOR
C
      IMPLICIT REAL*8 (A-H,O-Z)
      ST=0.D0
      SA=F(A)
      SB=F(B)
      N=2
      H=(B-A)*.5D0
      S=(SA+SB)*.5D0
      DO 10 I=1,7000
      T=0.D0
      DO 20 J=1,N-1,2
   20 T=T+F(A+H*J)
      S=S+T
      V=(S+T)*H*.6666666666666667D0
      IF (ABS(V-ST).LT.REL*ABS(ST)) GO TO 30
      ST=V
      N=N+N
   10 H=H*.5D0
   30 SIMP=V
      RETURN
      END
C
C
C
C
```

```
        SUBROUTINE FACTR(N,A,IP,NDIM)
C       ****************************************************************
C       SUBROUTINE TO FACTOR A MATRIX INTO A UNIT LOWER TRIANGULAR MATRIX
C       AND AN UPPER TRIANGULAR MATRIX USING THE GAUSS-DOOLITTLE ALGORITHM
C       PRESENTED ON PAGES 411-416 OF A. RALSTON--A FIRST COURSE IN
C       NUMERICAL ANALYSIS.  COMMENTS BELOW REFER TO COMMENTS IN RALSTONS
C       TEXT.     (MATRIX TRANSPOSED.
C       ****************************************************************
        IMPLICIT REAL*8 (A-H,O-Z)
        DIMENSION A(NDIM,NDIM), IP(NDIM)
        COMMON /SCRATM/ D(600)
        INTEGER R,RM1,RP1,PJ,PR
        IFLG=0
        DO 9 R=1,N
C
C       STEP 1
C
        DO 1 K=1,N
        D(K)=A(R,K)
1       CONTINUE
C
C       STEPS 2 AND 3
C
        RM1=R-1
        IF (RM1.LT.1) GO TO 4
        DO 3 J=1,RM1
        PJ=IP(J)
        ARJ=D(PJ)
        A(R,J)=ARJ
        D(PJ)=D(J)
        JP1=J+1
        DO 2 I=JP1,N
        D(I)=D(I)-A(J,I)*ARJ
2       CONTINUE
3       CONTINUE
4       CONTINUE
C
C       STEP 4
C
        DMAX=D(R)**2
        IP(R)=R
        RP1=R+1
        IF (RP1.GT.N) GO TO 6
        DO 5 I=RP1,N
        ELMAG=D(I)**2
        IF (ELMAG.LT.DMAX) GO TO 5
        DMAX=ELMAG
        IP(R)=I
5       CONTINUE
6       CONTINUE
        IF (DMAX.LT.1.D-10) IFLG=1
        PR=IP(R)
        A(R,R)=D(PR)
        D(PR)=D(R)
C
C       STEP 5
C
        IF (RP1.GT.N) GO TO 8
```

```
        ARJ=1.D0/A(R,R)
        DO 7 I=RP1,N
        A(R,I)=D(I)*ARJ
7       CONTINUE
8       CONTINUE
        IF (IFLG.EQ.0) GO TO 9
        PRINT 10, R,DMAX
        IFLG=0
9       CONTINUE
        RETURN
C
10      FORMAT (1H ,6HPIVOT(,I3,2H)=,E16.8)
        END
C
C
        SUBROUTINE SOLVE (N,A,IP,B,NDIM)
C       ****************************************************************
C       SUBROUTINE TO SOLVE THE MATRIX EQUATION LU*X=B WHERE L IS A UNIT
C       LOWER TRIANGULAR MATRIX AND U IS AN UPPER TRIANGULAR MATRIX BOTH
C       OF WHICH ARE STORED IN A.  THE RHS VECTOR B IS INPUT AND THE
C       SOLUTION IS RETURNED THROUGH VECTOR B.    (MATRIX TRANSPOSED.
C       ****************************************************************
        IMPLICIT REAL*8 (A-H,O-Z)
        INTEGER PI
        COMMON /SCRATM/ Y(600)
        DIMENSION A(NDIM,NDIM), IP(NDIM), B(NDIM)
C
C       FORWARD SUBSTITUTION
C
        DO 3 I=1,N
        PI=IP(I)
        Y(I)=B(PI)
        B(PI)=B(I)
        IP1=I+1
        IF (IP1.GT.N) GO TO 2
        DO 1 J=IP1,N
        B(J)=B(J)-A(I,J)*Y(I)
1       CONTINUE
2       CONTINUE
3       CONTINUE
C
C       BACKWARD SUBSTITUTION
C
        DO 6 K=1,N
        I=N-K+1
        SUM=0.D0
        IP1=I+1
        IF (IP1.GT.N) GO TO 5
        DO 4 J=IP1,N
        SUM=SUM+A(J,I)*B(J)
4       CONTINUE
5       CONTINUE
        B(I)=(Y(I)-SUM)/A(I,I)
6       CONTINUE
        RETURN
        END
```

APPENDIX C

APPROXIMATE EXPRESSION FOR THE CAPACITANCE OF A SMALL TUBULAR ANTENNA

Consider the tubular dipole shown in Fig. C–1(a). It consists of two perfectly conducting hollow tubes each of length h and radius a and separated by a distance 2s. The charge distribution along the dipole is rotationally symmetric. To compute the capacitance of the tubular dipole, consider the coplanar stripline geometry in Fig. C–1(b). It consists of two strips each of width h and length $2\pi a$ and separated by a distance 2s. The capacitance per unit length C_L of the coplanar stripline is given by [14]

$$C_L = \varepsilon_0 \frac{K(k')}{K(k)} \tag{C-1}$$

where

$$k = \frac{s}{s + h} \tag{C-2}$$

K(k) is the complete elliptic integral of the first kind [5] and $k' = (1 - k^2)^{1/2}$. The capacitance of the stripline in Fig. C–1(b) is obtained by multiplying C_L by the length $2\pi a$. Therefore, by approximating the tubular dipole in Fig. C–1(a) by the coplanar stripline in Fig. C–1(b), the dipole capacitance is

$$C = 2\pi a \varepsilon_0 \frac{K(k')}{K(k)} \tag{C-3}$$

The capacitance of a tubular monopole of height h and radius a and separated by a distance s above an infinite ground plane is given by twice the value in (C–3).
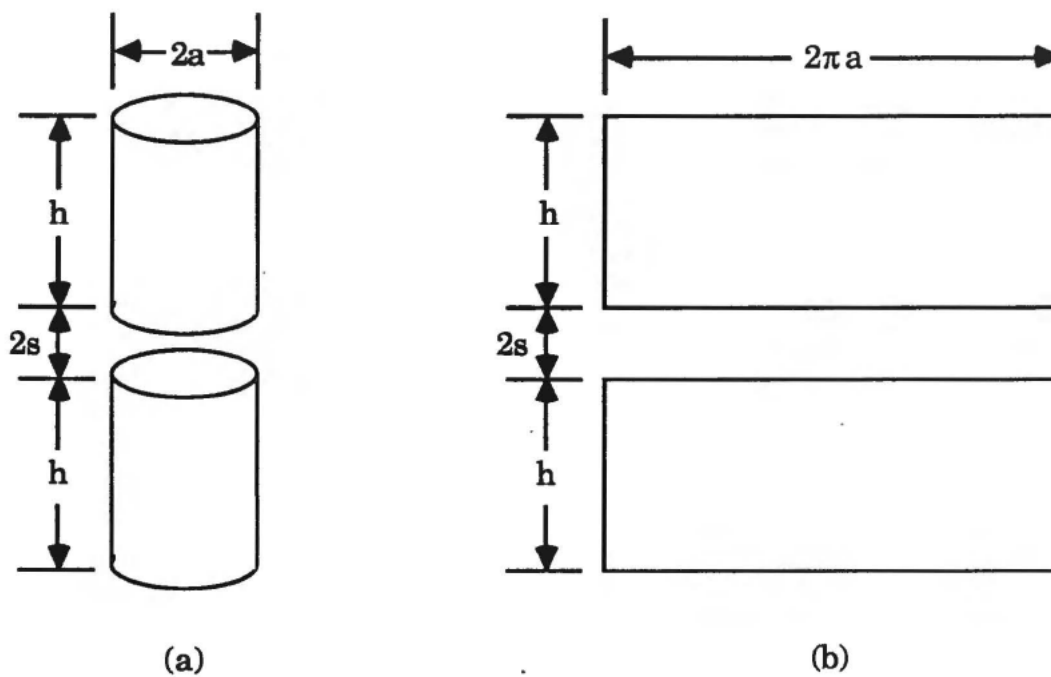
Figure C – 1 (a) Tubular dipole.
(b) Equivalent coplanar stripline.

INTERNAL DISTRIBUTION LIST

Code 10	
Code 101	Dr. K. Lima
Code 34	
Code 341	
Code 3411	
Code 3411	P. Bannister
Code 3411	J. Katan
Code 3411	W. Kraimer
Code 3411	E. Wolkoff
Code 3412	
Code 3412	R. Olesen
Code 3413	
Code 3413	K. White
Code 3421	
Code 3421	C. Aebli
Code 3421	G. Alvandian
Code 3421	Dr. J. Casey (5)
Code 3421	J. Comiskey
Code 3421	D. Esterquest
Code 3421	Dr. D. Fessenden
Code 3421	E. Gerhard
Code 3421	P. Gilles
Code 3421	K. Hafner
Code 3421	M. Josypenko
Code 3421	R. Koehler
Code 3421	M. McDonald
Code 3421	P. Mileski
Code 3421	C. Odams
Code 3421	B. Pease
Code 3421	D. Portofee
Code 3421	D. Rodriguez
Code 3421	D. Saleem
Code 3421	C. Spellman
Code 3422	
Code 34292	
Code 343	
Code 3431	
Code 3431	L. Dalsass
Code 3431	D. Dixon
Code 3431	M. Obara
Code 3431	N. Schade
Code 3491	
Code 3495	
Code 44	A. Bruno
Code 44	Dr. R. Kasper
Code 02111	A. Lotring
Code 02151	Library (New London) (3)
Code 02152	Library (Newport) (3)

External: 14
Internal: <u>56</u>
Total: 70

INITIAL DISTRIBUTION LIST

Addressee	No. of Copies
SPAWAR, PMW-50DP	1
SPAWAR, PMW-153DP	1
SPAWAR, PMW-153-2DP	1
NAVSEA, 395A	1
Prof. Rajeev Bansal, Dept. of Electrical and Systems Engineering U-157, University of Connecticut, Storrs, CT 06269	5
Dr. Val Liepa, EECS Department, University of Michigan, 3242 EECS, Ann Arbor, MI 48109	1
Dr. A. Kumar, AK Electromagnetic, Inc., 492 Westminster Ave., Dollard-des-Ormeaux, Quebec, Canada H9G 1E5	1
Gabriel Silberman, ARDEC, SCMAR-FSP-E, Bldg. 1530, Picatinny Arsenal, Picatinny, NJ 07806-5000	1
Dr. Harvey Schuman, Atlantic Research Corporation, 1721 Black River Boulevard, Rome, NY 13440	1
Prof. Donald Wilton, Department of Electrical Engineering, University of Houston, Houston TX	1